Master's Thesis of Natural Science

Evaluating the Applicability of the ^{3}H-^{3}He Age Tracer at a DNAPL Contaminated Site

DNAPL 오염 사이트에서의 ^{3}H-^{3}He 연령 추적자 적용 가능성 평가

February 2023

Graduate School of Seoul National University
College of Natural Sciences
School of Earth and Environmental Sciences

Ye Ji Kim

Evaluating the Applicability of the ^{3}H-^{3}He Age Tracer at a DNAPL Contaminated Site

Submitting a master's thesis of Natural Science

January 2023

Graduate School of Seoul National University
College of Natural Science
School of Earth and Environmental Science

Ye Ji Kim

Confirming the master's thesis written by
Ye Ji Kim
January 2023

Chair _____(Seal)
Vice Chair _____(Seal)
Examiner _____(Seal)

ABSTRACT

As a parameter for the flow of groundwater and transport of contaminants, groundwater age determined by the ^{3}H-^{3}He age tracer has been widely used. The conventional age calculation method has been based on the underlying assumption that the ^{3}He concentration is preserved along with the groundwater flow. However, this aspect can be violated within a DNAPL contaminated environment due to the preferential phase partitioning of noble gases to the DNAPL phase compared to water. Hence, the influence of phase partitioning to the age calculation was evaluated by comparing its influence to other influencing factors and applying a modified calculation method of the ^{3}H-^{3}He age tracer which takes the influence of noble gas phase partitioning into account. This method was applied to the DNAPL contaminated Namdong Industrial Complex (NIC) where noble gas and tritium concentrations were analyzed to determine the degree of phase partitioning and calculate the groundwater age. As a result, phase partitioning had a higher impact than the other influencing factors on groundwater age calculation for samples of low terrigenic source influence. The consideration of phase partitioning and the variation of the portion of tritiogenic helium influenced by phase partitioning varied the age calculation up to 4.6 years. This study suggested that phase partitioning of noble gases to the DNAPL phase has influence on the groundwater age calculation.

Keywords: DNAPL, ^{3}H-^{3}He age tracer, Noble gas, Phase partitioning

Student number: 2021-25787

TABLE OF CONTENTS

LIST OF FIGURES

LIST OF TABLES

1 INTRODUCTION

1.1 Research Background

Groundwater is an important natural resource that is utilized for various purposes including domestic, agricultural, and industrial uses. Hence, ensuring renewable supply of groundwater is of great importance (Famiglietti, 2014). However, industrial activities pose significant threats to groundwater contamination (i.e., oil spill, DNAPL contamination). To protect groundwater as a water resource, a thorough understanding of the origin and transport processes of pollutants in groundwater is needed (Schmoll et al., 2006).

Groundwater age analysis provides an insight to these processes of groundwater flow and contaminant transport behavior (Solomon et al., 1995; Morrison, 2000; Aeppli et al., 2010; Murphy et al., 2011). Based on the fact that urban area groundwater contaminations are considered to have occurred mostly during recent years (< 100 years), the ^{3}H-^{3}He age tracer, which is suitable for groundwater with an age up to 60 years, has been considered as an applicable tracer for the typical contaminated groundwater (Kipfer et al., 2002; Moeck et al., 2021). Researches have been conducted on contamination source allocation based on the reconstruction of the recharge period (Manning et al., 2005; Kaown et al., 2009; Mihajlov et al., 2020), verification of numerical groundwater models in order to define contaminant transport (Solomon et al., 1992; Murphy et al., 2011), and analyzation of the preferential groundwater flow in fractured aquifers to provide an extensive understanding of the potential contamination pathway (Amaral et al., 2010; Morgenstern et al., 2015).

The ^{3}H-^{3}He tracer is based on the radioactive decay of ^{3}H to ^{3}He with a half-life of 12.32 years (Unterweger et al., 1980). ^{3}H was generated by atmospheric thermonuclear bomb tests during the early 1960s and is bound in

meteoric water molecules ($^{1}H^{3}HO$) which reaches the groundwater table through precipitation (Kipfer et al., 2002). This ^{3}H within the groundwater goes through radioactive decay which thereafter produces ^{3}He, that is called tritiogenic ^{3}He ($=^{3}He_{tri}$).

The underlying assumption with the use of this age tracer is that the $^{3}He_{tri}$ concentration is preserved along the groundwater flow (Torgersen et al., 1977). However, there are events of violation to this assumption. In order to evaluate the age calculation deviation due to these factors their influence on the $^{3}He_{tri}$ concentration and ^{3}H-^{3}He age calculation have been made (Visser et al., 2007; Sultenfub et al., 2010; Mahara et al., 2014). Visser et al. (2007) observed degassing of ^{3}He due to the production of nitrogen gas during denitrification which was analyzed to cause a travel time uncertainty of 3 years. Mahara et al. (2014) found that the neglection of terrigenic ^{3}He ($=^{3}He_{ter}$), which is a term used during the calculation of $^{3}He_{tri}$, tends to overestimate the groundwater age. Both studies demonstrated that the application of a new age calculation method, which considered the influencing factors, provided more reasonable age calculations. Hence, the analyzation of influencing factors to the ^{3}H-^{3}He age calculation, which may be present in the field of interest, is necessary.

However, the deviation of ^{3}H-^{3}He age calculation within DNAPL contaminated sites due to the preferential phase partitioning of noble gases to the DNAPL phase than water has yet to be evaluated. Still, the ^{3}H-^{3}He age tracer has been applied and studied at numerous DNAPL contaminated sites. Murphy et al. (2011) investigated a site of multiple source zones using the ^{3}H-^{3}He age tracer to validate a numerical model for an enhanced understanding of the DNAPL transport in a complex aquifer system. Moek et al. (2021) also used the ^{3}H-^{3}He age tracer as an indicator of preferential flow paths for the contaminant transport and enlightened the fact that old groundwater was the source of contamination at this site. These studies have

applied the ^{3}H-^{3}He age tracer to evaluate groundwater flow within DNAPL contaminated sites without the consideration of noble gas phase partitioning to the DNAPL phase. However, there are various studies that have demonstrated the phase partitioning behavior of noble gases within a DNAPL-water system (Divine et al., 2003; Cho et al., 2020). Hence, verification of the influence of noble gas phase partitioning on groundwater age calculation using the ^{3}H-^{3}He tracer is needed.

1.2 Objectives and Scope

The main objective of this study is to evaluate the influence of noble gas phase partitioning to DNAPL on ^{3}H-^{3}He age calculation. To achieve this goal, this research was conducted based on the following procedures.

For the first step, possible influencing factors to the ^{3}H-^{3}He groundwater age calculation were evaluated. Comparison of the impact by phase partitioning relative to other influencing factors was conducted to verify the influence of phase partitioning on the groundwater age calculation. Hence, based on the equation that is used to derive the tritiogenic He ($^{3}He_{tri}$), the influencing factors were selected. These include the atmospheric noble gas determination, which depends on the excess air model selection, and the terrigenic source determination, which depends on the ratio between ^{3}He and ^{4}He of the terrigenic source (=R_{ter}).

Thereafter, ^{3}H-^{3}He groundwater age was calculated for varying cases. Cases were divided into two main categories: phase partitioning not considered (PPX), phase partitioning considered (PPY). For the PPX cases, the R_{ter} value was varied between the predetermined range for the study area. As for the PPY cases, groundwater age was calculated for two variables: (1) varying R_{terr} values, (2) extent of phase partitioning in terms of the location of DNAPL between the recharge and sampling point.

Finally, the impact of phase partitioning on the ^{3}H-^{3}He age calculation was evaluated by comparing the degree of groundwater age change due to the variation of the three influencing factors (atmospheric noble gas determination, terrigenic source determination, phase partitioning of noble gases to the DNAPL phase). This quantitative evaluation provided insight into whether phase partitioning significantly affected the groundwater age or not.

2 STUDY AREA

The study area is located at the Namdong industrial complex, Incheon, South Korea (Fig. 2-1a). While this place now stands as a representative industrial complex, before the 1980's it consisted of salt pans and mud flats (Fig. 2-2). After the Capital Region Plan had been announced, a land reclamation project was conducted from 1985 to 1997. Various factories were positioned thereafter which now all make up the industrial complex (Incheon Metropolitan City Museum, 2020).

At a regional scale, two streams are located to the South–East and South–West, each approximately 1 km from the study site, that are directly connected to the sea (Fig. 2-1b). As shown in Fig. 2-1c, the land use of the study site is mainly categorized into industrial use and impermeable roads.

The mean air temperature and mean total precipitation data for each month of Incheon throughout the recent 10 years (2012–2021) are represented in Fig. 2-3 (KMA, 2022). The highest temperature was 26.3℃ in August and the lowest temperature was -1.35℃ in January. The amount of precipitation during the wet season (July–September) was recorded to be a total of 589.4 mm which is 56.82% of the total annual precipitation, whereas the dry season (December–February) was analyzed to be 71.64 mm contributing to only 6.907% of the total annual precipitation. For this study, the wet season was defined as the three consecutive months of the highest total precipitation and the dry season was determined as vice versa.

Namdong-gu, which is the administrative district the study site is located in, has an area of 50.83 km^2. The total amount of water resources is 67,153,000 m^3/yr and the recharge amount is 7,456,000 m^3/yr, which indicates a recharge rate of 11.1% (Korea Water Resource Corporation, 2005). This low rate is consistent with the fact that more than 40% of the Incheon inland area (where Namdong-gu is situated) consists of urban districts with

the high possibility of surface runoff (Korea Water Resource Corporation, 2005).

Boring investigations were conducted at fifteen groundwater monitoring wells (NDMW-09–NDMW-13, MW-1–MW-5, BH-1–BH-3, DJ-1) which have a length ranging between 50 to 52 m (Table 2-1). Based on the investigation results of these monitoring wells, cross-sectional geological maps were obtained. Fig. 2-4 shows the overview of the sections analyzed represented as lines, and Fig. 2-5 – Fig. 2-7 are the respective cross-sections. The study site mainly consisted of 4 layers: landfill (silty sand), sedimentary layer (sand and silty clay), weathered soil (silty sand), and bedrock (Mica Schist). The characteristic layer of landfill extends to a depth varying between 0 to 12 m, where NDMW-09 is the thickest and NDMW-12 is the thinnest. Below, the sedimentary layer is 4–16 m thick which is followed by the weathered soil layer that has a thickness of 2–10 m. Among the monitoring wells shown in Fig. 2-4, all wells are bedrock wells except for the NDW wells which are alluvial wells (Korea Environment Corporation, 2020).

The thickness of the unsaturated zone was relatively thin, based on the groundwater levels of the study site which ranged between 0.935 m, b.g.l. and 1.420 m, b.g.l. among the monitoring wells that were sampled on 4th April, 2021. Detailed information on the monitoring wells is summarized in Table 2-1. Based on the elevation and groundwater level obtained, the local groundwater flow was determined to be as shown in Fig. 2-8.

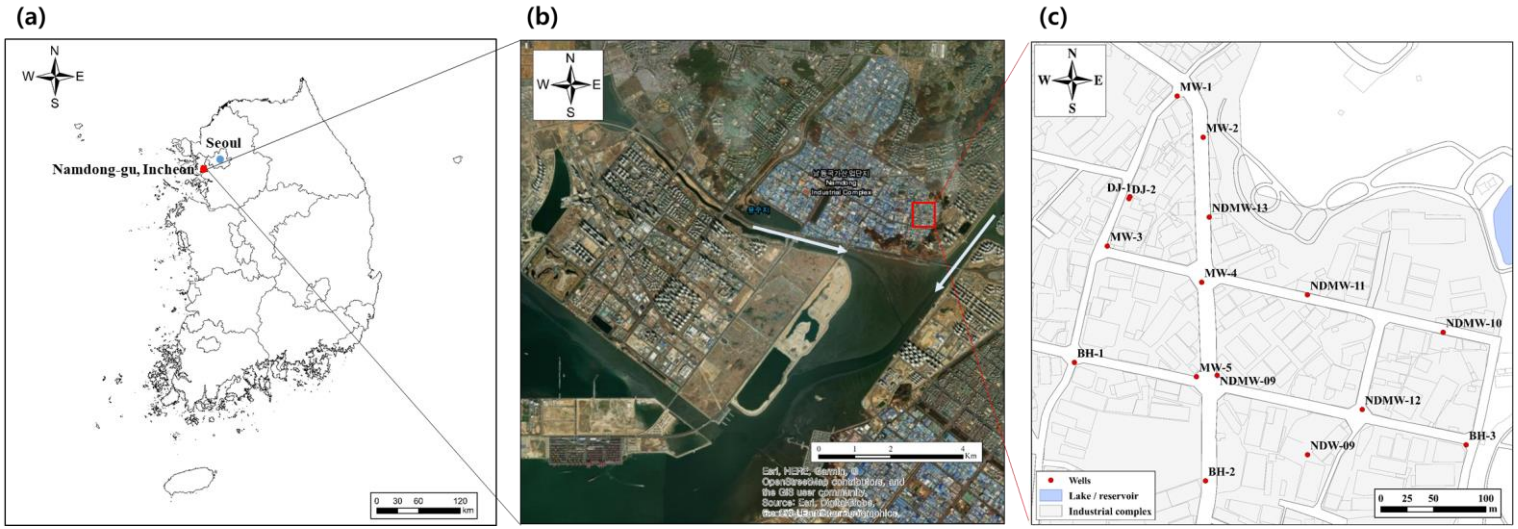

Fig. 2-1 (a) Map of the Republic of Korea, (b) satellite view of Incheon with a red box indicating the location of the study site, (c) land use and location of wells within the study site.

Fig. 2-2. Change in Namdong area by time: (a) Land use map at 1972 (Incheon Metropolitan City Museum, 2020), (b) Satellite view at 1985/12 (Google Earth), (c) Satellite view at 2020/12 (Google Earth). The white stars indicate the location of the study site.

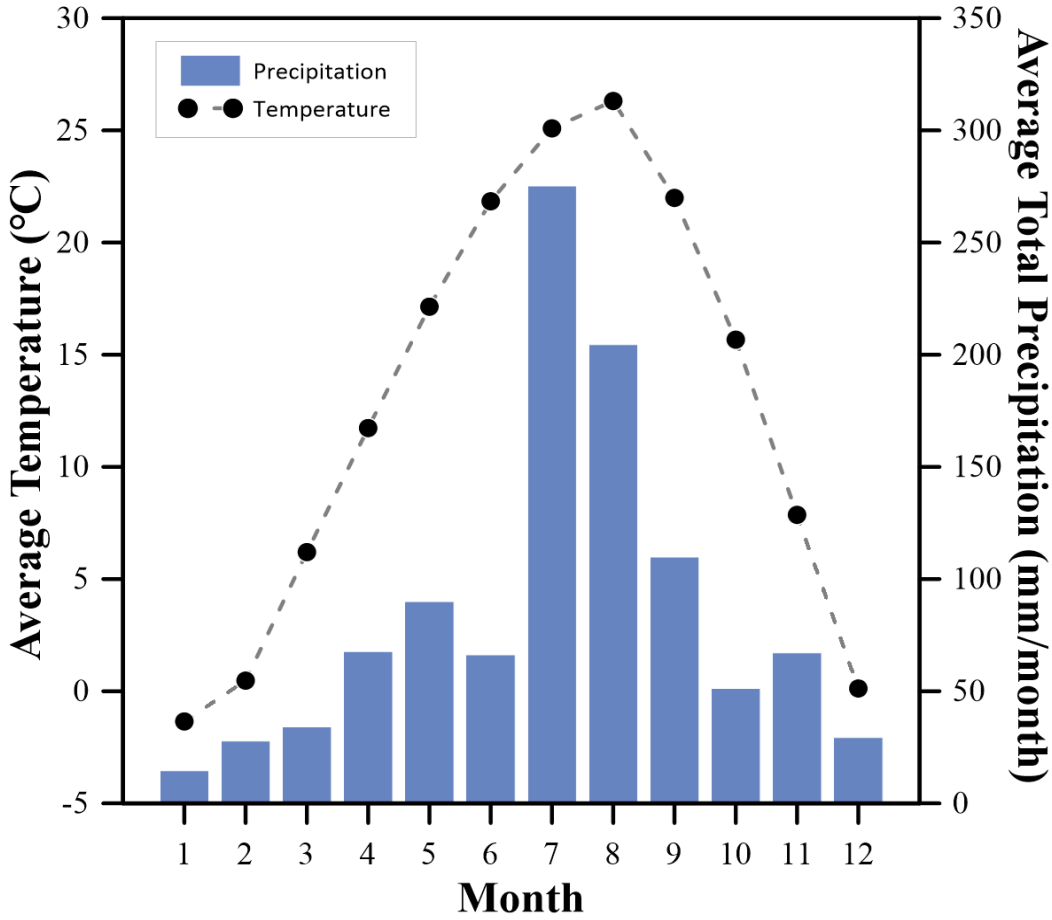

Fig. 2-3. Monthly averaged temperature and averaged total precipitation of Incheon for 10 years from 2012 to 2021. The black dot line represents the mean temperature and the blue bar shows the mean total precipitation.

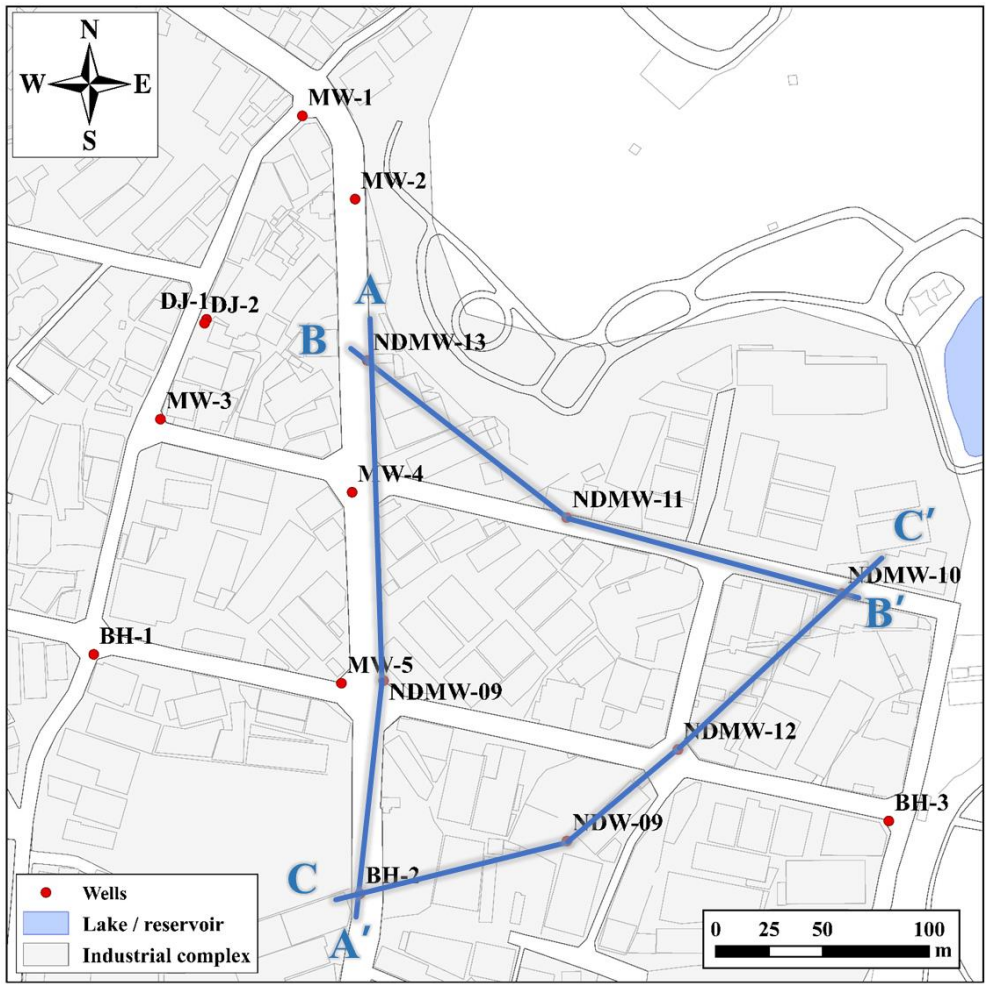

Fig. 2-4. The representation of the areas of cross-sectional analysis.

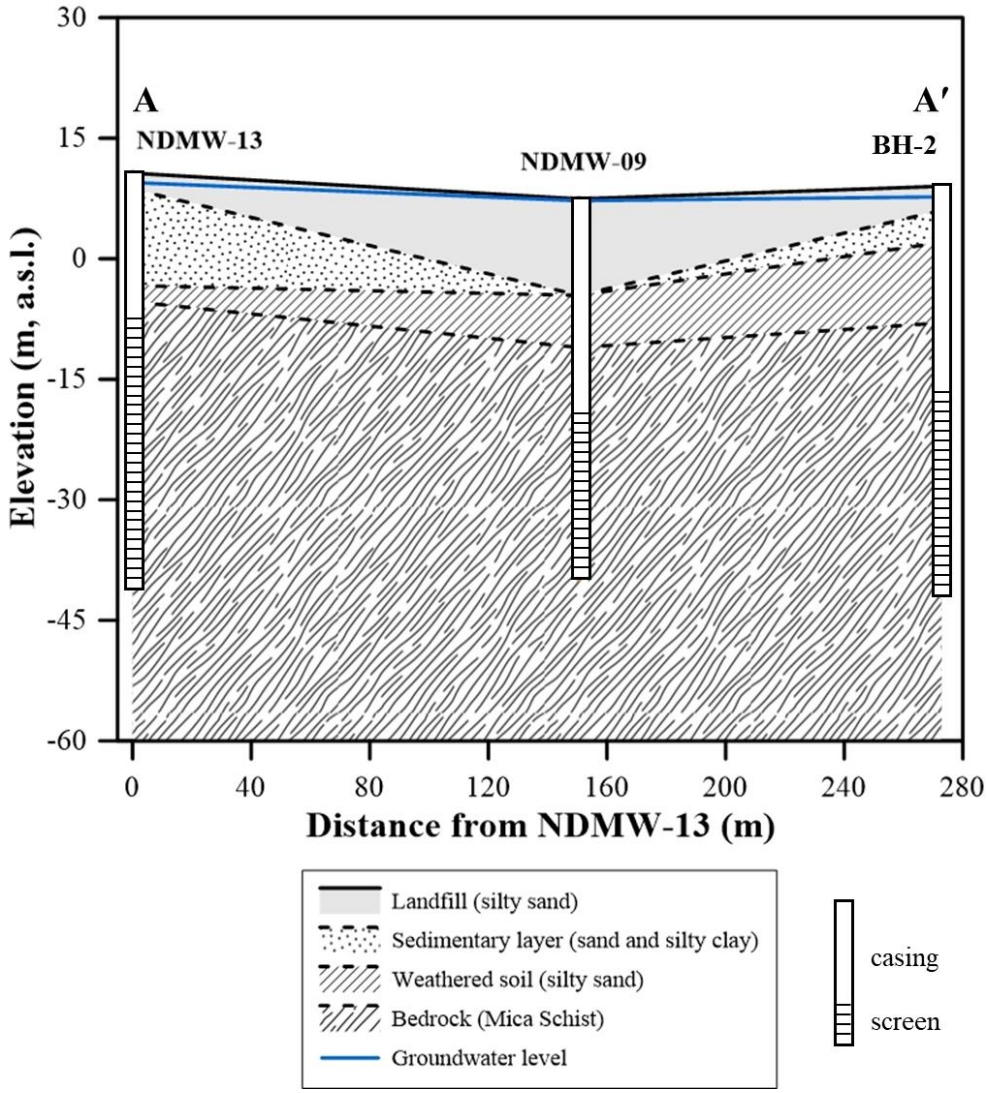

Fig. 2-5. Cross-sectional stratigraphy of line A-A′.

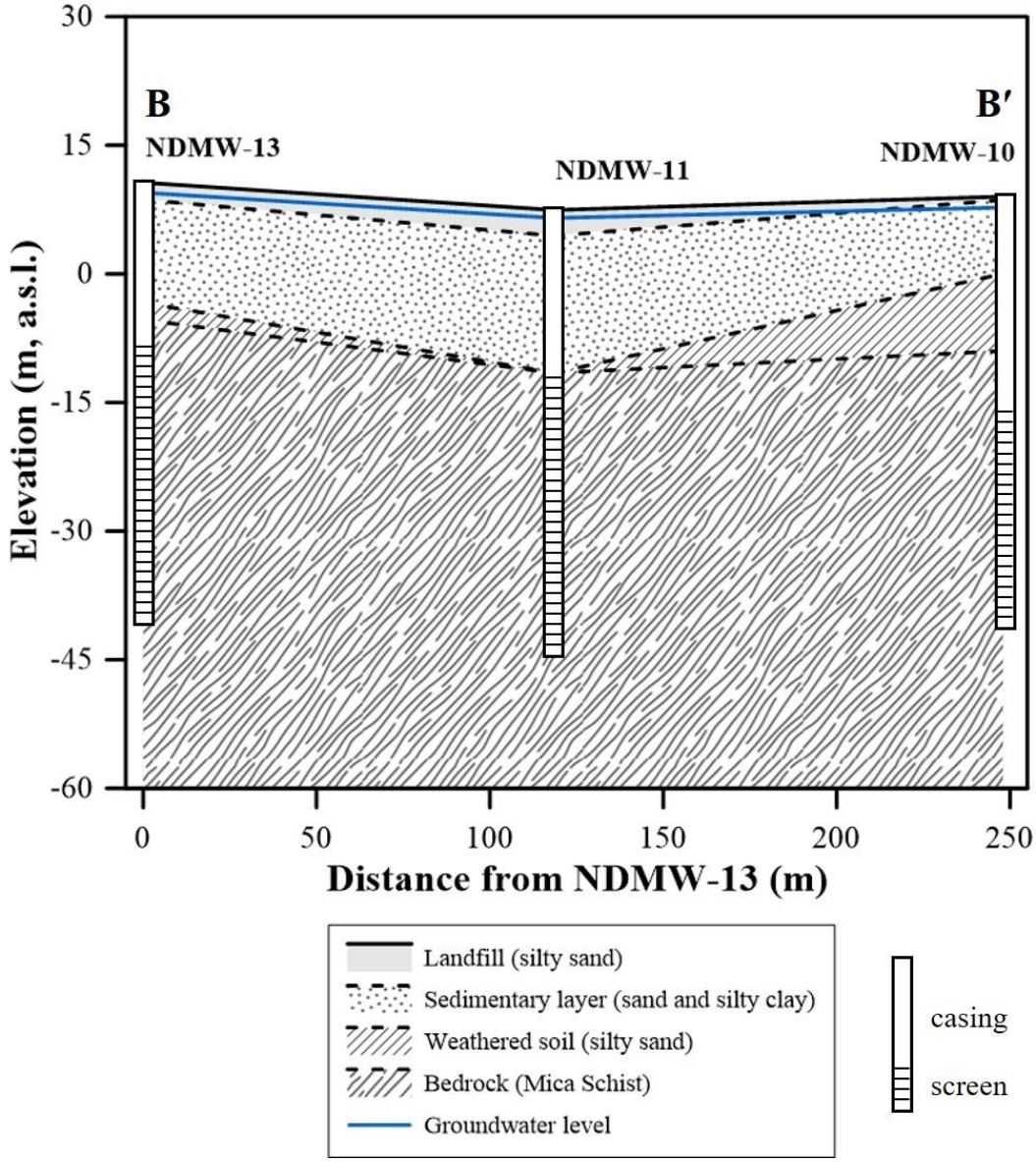

Fig. 2-6. Cross-sectional stratigraphy of line B-B′.

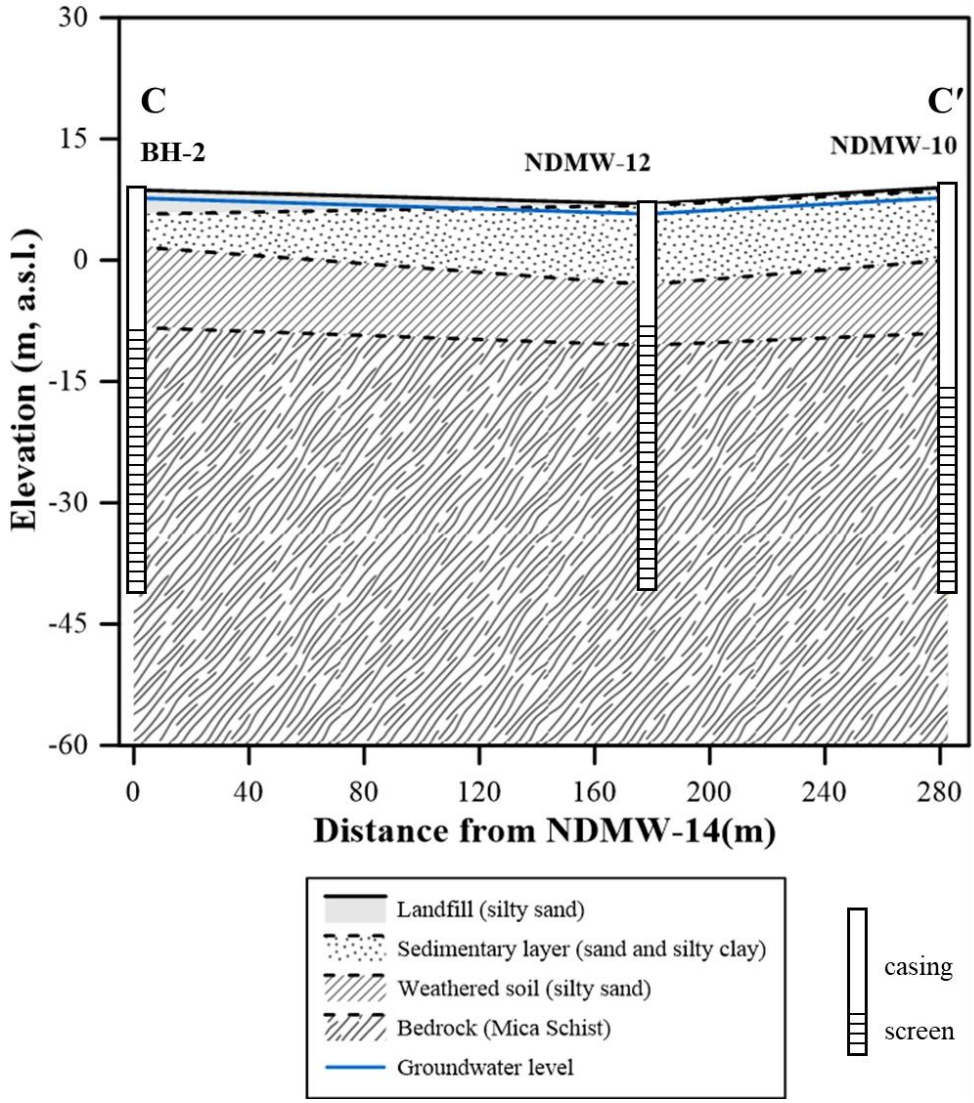

Fig. 2-7. Cross-sectional stratigraphy of line C-C′.

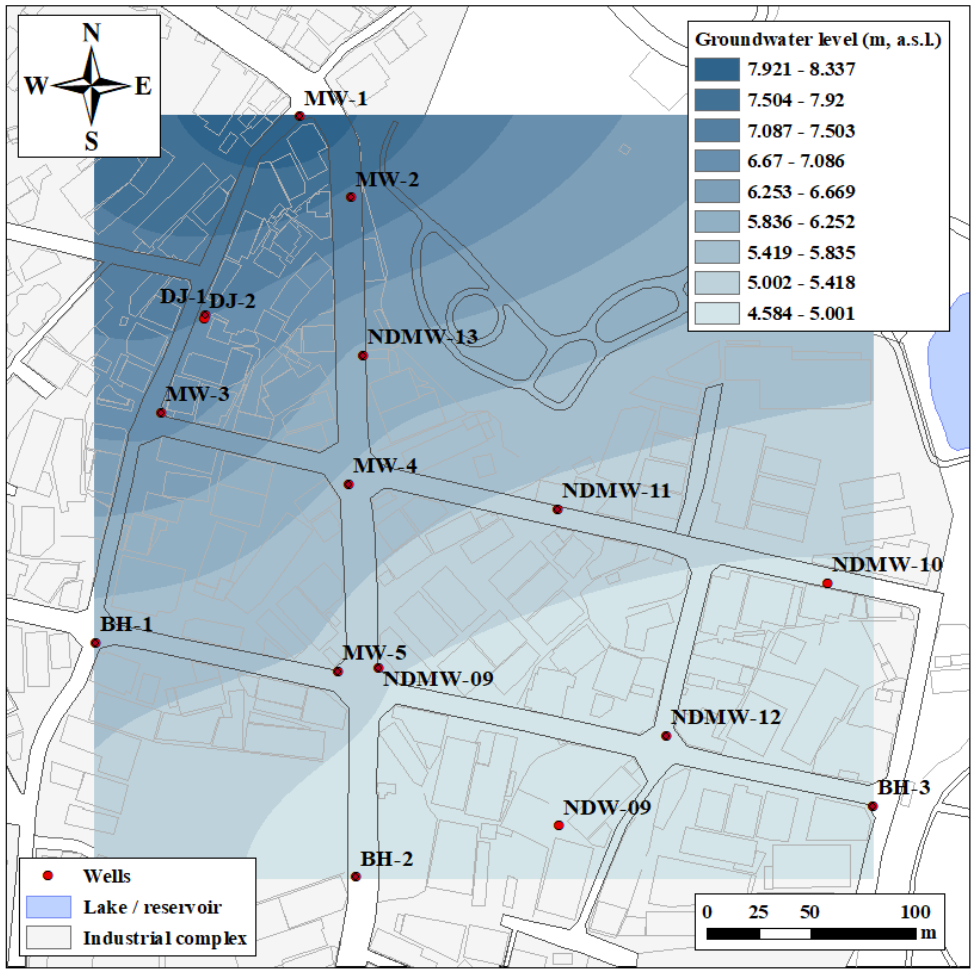

Fig. 2-8. Groundwater level at a regional scale on 4th April, 2022

Table 2-1. General information (elevation, well depth) on monitoring wells, and data (groundwater level, sampling depth) obtained during the sampling campaign conducted on September 2021 and April 2022.

Well	Elevation (m, a.s.l.)	Groundwater level (m, b.g.l.)		Sampling depth (m, b.g.l.)
		September 2021	April 2022	
NDMW-09	8.645	1.420	1.790	25
NDMW-10	9.021	1.270	-	32
NDMW-11	7.450	0.935	1.260	18
NDMW-12	6.979	1.255	1.680	33
NDMW-13	10.653	1.170	1.535	39
BH-1	12.67	-	5.250	28
BH-2	8.45	-	1.640	38
BH-3	8.36	-	1.700	32
MW-1	16.86	-	8.080	34
MW-2	15.46	-	3.240	32
MW-3	11.57	-	3.180	30
MW-4	8.25		0.900	30
MW-5	9.09	-	1.720	25

3 METHODS AND MATERIALS

3.1 Sampling and Data Acquisition

Two sampling campaigns were conducted between 16th–17th September, 2021 (September 2021) and 4th–5th April, 2022 (April 2022). Wells specified in Fig. 2-4 were sampled using a submersible and controllable quantitative pump (MP1, Grundfos, Denmark) connected to a polyethylene pipe. In order to minimize cross contamination, the attached hose was changed for each well. The sampling depth for each well corresponded to the depth of the highest DNAPL concentration which was determined through previous groundwater quality analysis. Well information and the measured groundwater level and sampling depth at the time of sampling are listed in Table 2-1.

The chemical parameters (pH [-], temperature [℃], oxidation-redox potential [mV], electrical conductivity [μS/cm], DO [mg/L]) were measured on-site by the multiparameter instrument (ProDSS Multiparameter Digital Water Qua1lity Meter, YSI, USA) with the probes for conductivity, ORP, and pH (YSI probe 626902, 626900, and 626903, YSI, USA). Prior to sampling, purging was carried out more than three times of the well volume until the measured chemical parameters were stabilized.

Noble gas concentrations were obtained for ^{3}H-^{3}He groundwater age and phase partitioning analysis. Noble gas samples were collected using the copper tube method following the Utah Noble Gas Lab's protocol (https://noblegaslab.utah.edu/). The procedure involved the connection of the PE tube to a flexible tube which was then connected to two 28 cm^{3} copper tubes sequentially. After groundwater purging, the two stainless-steel clamps were tightened assuring air bubbles, which could act as contamination to the samples, were not present within the sealed section. A schematic figure of the noble gas sampling procedure is depicted in Fig. 3-1. Analyzation of the samples were conducted at the University of Utah Noble Gas Lab

(Aeschbach-Hertig and Solomon, 2013; Solomon et al., 2015). As for the analysis method, a high-vaccum closed system was used to extract dissolved gases from the samples and transferred these gases into a stainless steel flask. This flask was thereafter connected to a mass spectrometry line which removes water vapor and condensable gases using cryogenic traps and getters respectively. He was analyzed using a sector-field mass spectrometer (Mass Analyser Products, model 215-50), and the remaining noble gas species, including Ne, Ar, Kr, and Xe, and their isotopes were analyzed with a quadrupole mass spectrometer (Stanford Research Systems RGA300). The measurement error is ± 1% for helium, and ± 1% to ± 5% for the other noble gases (Mannings et al., 2005).

Last but not least, tritium(^{3}H) concentrations were used to calculate the groundwater age. For ^{3}H analysis, groundwater was sampled in a 1 L High Density Polyethylene (HDPE) bottle with no headspace and airtight to prevent evaporation. Analyzation was conducted at the Environmental Isotope Laboratory of Waterloo University which used the liquid scintillation counting (LSC) method for the quantification of tritium. The detection limit is 0.8 TU and the precision is ± 0.8 TU. A summary of the chemical parameters analyzed in laboratories, the institute at which they were analyzed, the devices that were used, and the precision of analysis are shown in Table 3-1.

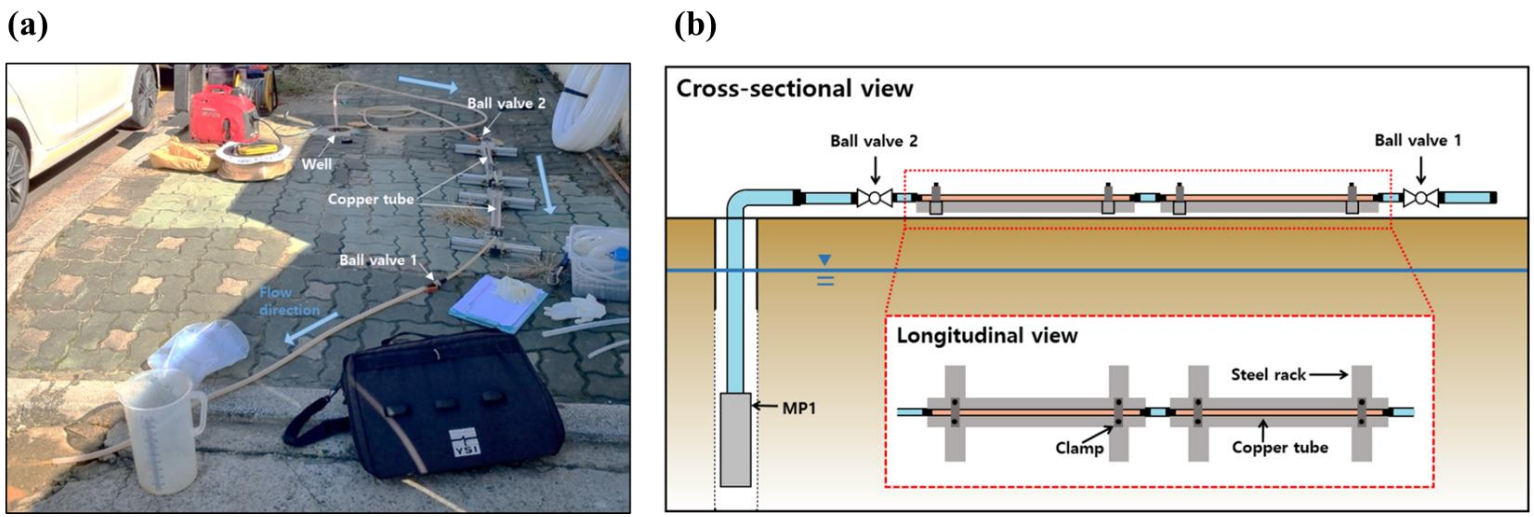

Fig. 3-1. The water sampling procedure to interpret the noble gas concentration: (a) field setting, (b) schematic diagram (modified from Cho, 2020).

Table 3-1. Summary of the institute, device, and precision of analysis for each analyzed factor

Analyzed factor	Institute	Device	Precision
Noble gases	Noble Gas Lab, University of Utah, USA	Sector-field MS & Quadrupole MS (RGA300)	± 1% for He ± 5% for Ne, Ar, Kr, Xe
Tritium	Environmental Isotope Laboratory, University of Waterloo, Canada	Liquid Scintillation Counting (LSC)	± 0.8 TU

3.2 Influence Factors for Groundwater Age Calculation

The origin of noble gases within the groundwater is either atmospheric or non-atmospheric. Noble gas concentrations from atmospheric origin can be further subdivided into air equilibrated concentration (C_{eq}, [ccSTP/g]) and excess air concentration (C_{ex}, [ccSTP/g]), while the non-atmospheric origin consists of terrigenic concentration (C_{ter}, [ccSTP/g]) and tritiogenic concentration (C_{tri}, [ccSTP/g]). The subdivision of each noble gas into its origins for typical shallow groundwater is shown in Table 3-2. The total concentration of a noble gas species measured within a groundwater sample is hence the sum of the concentrations from each origin, which can be expressed by the following equation.

$$C_m^i = C_{eq}^i + C_{ex}^i + C_{ter}^i + C_{tri}^i \qquad \text{(Eq. 3-1)}$$

where i is the type of noble gas (He, Ne, Ar, Kr, Xe), and C_m^i is the total concentration of i in the water sample measured [ccSTP/g].

For groundwater age calculation, $^3He_{tri}$ is used which can be derived from Eq. 3-1 as the following equation

$$C_{tri}^{3He} = C_m^{3He} - (C_{eq}^{3He} + C_{ex}^{3He} + C_{ter}^{3He}) \qquad \text{(Eq. 3-2)}$$

Therefore, the calculation of $^3He_{tri}$ is influenced by the determination of the atmospheric concentration (equilibrium and excess concentration) and the estimation of the terrigenic source. These two influencing factors are common sources of error to the calculation of groundwater age and have been verified of their impact on groundwater age calculation (Peeters et al., 2003; Visser et al., 2007; Mahara et al., 2014; Visser et al., 2014).

In addition to these common influencing factors, the effect of phase partitioning to DNAPL is evaluated in this study. Divine et al. (2003)

demonstrated that noble gases show partitioning characteristics between DNAPL and water at a laboratory scale experiment. Based on this fact, Cho et al. (2020) determined the poassible range of residual DNAPL within an area which was analyzed to have high concentrations of TCE. In similarity, NIC has also been shown to be contaminated with DNAPL which has been clarified through groundwater sampling. Hence, there is the possibility of residual DNAPL present in the aquifer which induces phase partitioning of noble gases. In order to evaluate the significance of this additional factor, comparison with the groundwater age deviation induced by the previously mentioned two influencing factors is made.

Table 3-2. Sources (equilibrium, excess, terrigenic, tritiogenic) of each noble gas component (He, Ne, Ar, Kr, Xe) typical for shallow groundwater.

	Equilibrium (eq)	Excess (ex)	Terrigenic (ter)	Tritiogenic (tri)
^{3}He	O	O	O	O
^{4}He	O	O	O	X
Ne	O	O	X	X
Ar	O	O	X	X
Kr	O	O	X	X
Xe	O	O	X	X

3.2.1 Atmospheric concentration determination

For the solubility equilibrium component (C_{eq}), the empirical equation derived by Weiss (1970, 1971) and Weiss and Kyser (1978) was used for He, Ne, Ar, and Kr. This equation is a function of the temperature, salinity, and pressure.

$$C_{eq}^{i} = \exp\left(t_1 + t_2 \cdot \frac{100}{T} + t_3 \cdot \ln\left(\frac{T}{100}\right) + t_4 \cdot \frac{T}{100} + S \cdot \left[s_1 + s_2 \cdot \frac{T}{100} + s_3 \cdot \left(\frac{T}{100}\right)^2\right]\right) \times \frac{p_{tot} - e_w}{(p_{norm} - e_w) \cdot 1000} \quad \text{(Eq. 3-3)}$$

where C_{eq}^{i} is the equilibrium concentration of noble gas *i* [ccSTP/g], p_{tot} and p_{norm} are the total local atmospheric pressure [atm] and reference pressure (= 1 atm) [atm] respectively, e_w is the water vapor pressure [atm], and t_1, t_2, t_3, t_4, s_1, s_2, and s_3 are coefficients that differ by the type of noble gas and are shown in Table 3-3.

Unlike the equilibrium component, the excess component concentration (C_{ex}^{i}) is determined between four excess air models: UA (Unfractionated Air), PR (Partial Re-equilibrium), PD (Partial Degassing), and CE (Closed-system Equilibrium) model (Andrews and Lee, 1979; Stute et al., 1995; Lippmann et al., 2003; Aeschbach-Hertig et al., 2000). These models differ in the way of interpreting the fractionation of the entrapped air during groundwater recharge.

The UA model assumes complete dissolution of small air bubbles trapped in soil pores which implies that excess air has the same composition as the atmospheric air (Andrews and Lee, 1979).

$$C_w^i = C_w^i + AC_a^i = C_{eq}^i + C_{eq}^i AH_i \qquad \text{(Eq. 3-4)}$$

where C_w^i is the concentration of i in the water sample [ccSTP/g], C_a^i is the concentration of i in the air [ccSTP/g], C_{eq}^i is the concentration of i in air equilibrated water [ccSTP/g], A is the excess air volume per volume of water [-], and H_i is the Henry's constant of i [-].

The PR model is an extension of the UA model, where entrapped air bubbles are initially completely dissolved, but later lost depending on molecular diffusion across the water table (Stute et al., 1995).

$$C_w^i = C_{eq}^i + AC_a^i e^{\left(-F_{PR}\frac{D_i}{D_{Ne}}\right)} = C_{eq}^i + C_{eq}^i AH_i e^{\left(-F_{PR}\frac{D_i}{D_{Ne}}\right)} \qquad \text{(Eq. 3-5)}$$

where F_{PR} is the degree of re-equilibrium for the PR model, and D_i is the diffusion coefficient for i [cm^2/s].

The PD model is similar to the PR model, but assumes the diffusive gas loss affects the total gas concentration rather than the excess air solely (Lippmann et al., 2003).

$$C_w^i = C_{eq}^i e^{\left(-F_{PD}\frac{D_i}{D_{Ne}}\right)} + C_{eq}^i AH_i e^{\left(-F_{PD}\frac{D_i}{D_{Ne}}\right)} \qquad \text{(Eq. 3-6)}$$

where F_{PD} is the degree of re-equilibrium for the PD model [-].

The CE model is conceptually different from the previous models in that it does not assume complete dissolution of initial entrapped air, but only partial dissolution depending on the solubility of the noble gases (Aeschbach-Hertig et al., 2000).

$$C_w^i = C_{eq}^i + C_{eq}^i \frac{(1-F)AH_i}{1+FAH_i} \qquad \text{(Eq. 3-7)}$$

where F is the ratio of the final and initial air bubble volume [-].

In order to determine the best fit model for each groundwater sample, the inverse modeling technique based on error weighted least squares fitting and the χ^2-test were conducted through the Matlab program Noble90 (Aeschbach-Hertig et al., 1999). Based on Eqs. 3-4–3-7, the fitting was carried out to estimate the unknown parameters (temperature (*T*, [°C]), salinity (*S*, [PSU]), pressure (*P*, [atm]), *A*, and *F*) with the known parameters (the concentration of Ne, Ar, Kr, and Xe). After the estimation of the parameters, the best-fit result to the observed concentrations was determined through the minimization of the χ^2 value which is calculated by (Aeschbach-Hertig et al., 1999)

$$\chi^2 = \sum_i \frac{(C_i^{meas} - C_i^{mod})^2}{\sigma_i^2} \qquad \text{(Eq. 3-8)}$$

where C_i^{mod} is the modeled concentration of *i* [ccSTP/g], C_i^{meas} and σ_i are the measured concentration of *i* [ccSTP/g] and its experimental error [ccSTP/g] respectively.

Based on the resulting noble gas component separation using Eqs. 3-3–3-7, the atmospheric and excess air origin noble gas concentration can be quantified. In cases where more than one excess air model is determined reasonable, the application of each model results in different tritiogenic helium ($^3He_{tri}$) concentration. Hence, the selection of the best fit excess air model may alter the calculation of $^3He_{tri}$.

Table 3-3. Coefficients of each noble gas element for the solubiltiy equilibrium calculation (Weiss, 1970; Weiss, 1971; Weiss and Kyser, 1978).

	t_1	t_2	t_3	t_4	s_1	s_2	s_3
He	167.2178	216.3442	139.2032	22.6202	0.04478	0.023541	0.0034266
Ne	170.6018	225.1946	140.8863	22.6290	0.12711	0.079277	0.0129095
Ar	178.1725	251.8139	145.2337	22.2046	0.03873	0.017171	0.0021281
Kr	112.684	153.5817	74.4690	10.0189	0.01121	0.001844	0.0011201

3.2.2 Terrigenic source determination

The terrigenic source of noble gases within the groundwater originates from different geochemical reservoirs of the solid earth including the Earth's mantle and crust. In the case of helium, ^4He is from deep aquifers due to the alpha-decay process of U/Th within the bedrock (Torgersen, 1989). As for the ^3He concentration, radioactive decay process contribution is insignificant and the major quantity is of 'primitive' ^3He during accretion (Mamyrin and Tolstikhin, 1984; Ballentine et al., 2002). Due to the characteristic isotope geochemistry, the terrigenic source of helium is represented as a uniform $^3He/^4He$ ratio (Kipfer et al., 2002). The value of this ratio varies with the composition of the bedrock.

The typical value for the R_{ter} is 2.00E-8 (Mamyrin and Tolstikhin, 1984). However, this value is not guaranteed to represent this study area since there is no previous study which analyzed the terrigenic source at this site. Hence, a range of values for R_{ter} was determined. The minimum value was put to be 0 which represents no $^3He_{ter}$ concentration. For the maximum value, the relationship between Ne/He and $^3He/^4He$ of the samples were analyzed and the y-intercept of the regression line was determined to be the maximum value of R_{ter} for the study area. This is based on the fact that when Ne/He approaches zero, that indicates atmospheric gas contribution becomes negligible compared to the terrigenic contributions (Peeters et al., 2003).

3.2.3 Phase partitioning between DNAPL and water

Phase partitioning is defined as the concentration separation of a species between two immiscible substances (Bouchard et al., 1989; Brusseau, 1992). The typical phase partitioning is observed between the gas-liquid and liquid-liquid phases (Brusseau et al., 2003). The constants that describe the characteristics of these two systems are the Henry's constant and partitioning coefficient respectively. The following equations represent the Henry's constant for a gas-water system, and the partitioning coefficient for a DNAPL-water system.

$$K_i^d = \frac{C_{i,gas}}{C_{i,water}} \quad \text{(Eq. 3-9)}$$

$$D_{i,DNAPL-water} = \frac{C_{i,DNAPL}}{C_{i,water}} = \frac{K_{i,water}}{K_{i,DNAPL}} \quad \text{(Eq. 3-10)}$$

where K_i^d is the dimensionless Henry's constant [-], $D_{i,DNAPL-water}$ is the partitioning coefficient of *i* between DNAPL and water [-], $C_{i,}$ is the concentration [ccSTP/g], and the subscripts *d*, *gas*, *water*, *DNAPL* each correspond to dimensionless, gas phase, water phase, and DNAPL phase.

For the closed system, the noble gas composition of the water after equilibration with DNAPL can be calculated by

$$[i]_T = [i]_{DNAPL} + [i]_{water} \quad \text{(Eq. 3-11)}$$

$$\begin{aligned}[i]_{DNAPL} &= [i]_T \left(\frac{V_{water}\rho_{water}}{V_{DNAPL}\rho_{DNAPL}} \frac{K_{i,DNAPL}^m}{K_{i,water}^m} + 1 \right)^{-1} \\ &= [i]_T \left(\frac{V_{water}\rho_{water}}{V_{DNAPL}\rho_{DNAPL}} \cdot \frac{1}{D_{i,DNAPL-water}} + 1 \right)^{-1}\end{aligned} \quad \text{(Eq. 3-12)}$$

$$[i]_{water} = [i]_T \left\{ 1 - \left(\frac{V_{water}\rho_{water}}{V_{DNAPL}\rho_{DNAPL}} \cdot \frac{1}{D_{i,DNAPL-water}} + 1 \right)^{-1} \right\} \quad \text{(Eq. 3-13)}$$

where $[i]$ is the number of moles of noble gas *i* [mol], *V* is volume [L], ρ is density [kg/L], *K* is Henry's Constant [atm kg mol^{-1}], and the subscripts *DNAPL*, *water*, and *T* correspond to the DNAPL phase, water phase, and total summation of these two. In other words, $[i]_T$ is the initial noble gas concentration of the water phase.

To determine the degree of fractionation, at least two of the atmospheric derived noble gas elemental isotopes (^{20}Ne, ^{36}Ar, ^{84}Kr, ^{132}Xe) have to be analyzed based on their partitioning coefficients. Divine et al. (2003) experimentally determined the partitioning coefficients for He and Ne within the PCE-water and TCE-water system at 20°C. However, analysis of other noble gas species were limited due to experimental difficulties. Hence, for an extensive analyzation of the phase partitioning behavior, the partitioning coefficients for the heavy oil, which are assumed to provide meaningful results for the NAPL analyzation (Cho et al., 2020; Kharaka and Specht, 1988), were used (Table 3-4).

Based on these partitioning coefficients, the best fit relative volume ratio of water to DNAPL ($\frac{V_{water}}{V_{DNAPL}}$) could be determined for each sample. This was thereafter used to derive the degree of fractionation for the atmospheric derived noble gas elements that were used for the analysis (i.e., $[Ne]_{water}/[Ne]_T$, $[He]_{water}/[He]_T$ named as F_{Ne} and F_{He} respectively in Chapter 3.3.2).

Table 3-4. Partition coefficients of He and Ne for a PCE-water and TCE-water system at 20°C (Divine et al., 2003), and partition coefficients of noble gases (He, Ne, Ar, Kr, Xe) for a heavy oil-water system at 12°C (Kharaka and Specht, 1988).

	PCE [-]	TCE [-]	Heavy oil [-]
He	1.28	2.42	1.48
Ne	1.84	3.24	1.05
Ar	-	-	3.93
Kr	-	-	6.22
Xe	-	-	11.93

3.3 ^{3}H-^{3}He Age Tracer Analysis

3.3.1 Basic Calculation Method

Based on the law of radioactive decay, the ^{3}H-^{3}He groundwater age can be calculated by (Tolstikhin and Kamenskiy, 1969)

$$\tau = \frac{1}{\lambda} \ln\left(1 + \frac{^3He_{tri}}{^3H}\right) \quad \text{(Eq. 3-14)}$$

where τ is the groundwater age [yr], λ is the decay constant of tritium (half-life of 12.32 yr, λ = 0.05626 yr^{-1}), $^3He_{tri}$ and ^3H are the measured concentrations of tritiogenic ^{3}He and ^{3}H within the water sample [TU], respectively.

The ^{3}H concentration is obtained by the groundwater sample analysis conducted as described in Chapter 3.1. As for the $^3He_{tri}$ concentration, it is calculated based on Eq. 2-2 as mentioned previously. For the calculation of $^3He_{tri}$, the specific component separations of Ne and ^{4}He are needed. The reason for the use of Ne and ^{4}He for the calculation of ^{3}He is due to the fact that Ne typically has only two soruces (eq, ex), ^{4}He has three sources (eq, ex, ter), and ^{3}He has four sources (eq, ex, ter, tri). Hence, the component separation of equilibrium and excess air by Ne and terrigenic component by ^{4}He can provide parameters for the calculation of $^3He_{tri}$. The source separation of Ne and ^{4}He can be expressed as

$$Ne_m = Ne_{eq} + Ne_{ex} \quad \text{(Eq. 3-15)}$$

$$\begin{aligned} ^4He_m &= {}^4He_{eq} + {}^4He_{ex} + {}^4He_{ter} \\ &= {}^4He_{eq} + L_{ex} \cdot Ne_{ex} + {}^4He_{ter} \end{aligned} \quad \text{(Eq. 3-16)}$$

where L_{ex} is the ratio between He and Ne of the excess air (= (He/Ne)$_{ex}$ [-]). L_{ex} has a value that ranges below 0.288, which is the maximum value

corresponding to the atmospheric composition ratio, and varies depending on the excess air model and excess air volume (Kipfer et al., 2002). The combination of Eqs. 3-1–3-2 and Eqs. 3-15–3-16 and the relation between ^{3}He and ^{4}He results the following.

$$
\begin{aligned}
{}^3He_m = R_{eq} \cdot {}^4He_{eq} + R_{ex} \cdot L_{ex} \cdot \left(Ne_m - Ne_{eq}\right) + R_{ter} \\
\cdot \Big({}^4He_m - {}^4He_{eq} - L_{ex} \\
\cdot \left(Ne_m - Ne_{eq}\right)\Big) + {}^3He_{tri}
\end{aligned}
\qquad \text{(Eq. 3-17)}
$$

$$
\begin{aligned}
{}^3He_{tri} = {}^4He_m \cdot R_m - R_{eq} \cdot {}^4He_{eq} - R_{ex} \cdot L_{ex} \cdot \\
\left(Ne_m - Ne_{eq}\right) - R_{ter} \cdot \{ {}^4He_m - {}^4He_{eq} - L_{ex} \cdot \\
\left(Ne_m - Ne_{eq}\right)\}
\end{aligned}
\qquad \text{(Eq. 3-18)}
$$

where R is the helium isotopic ratio (= ^{3}He/^{4}He [-]). R_{ex} has a value of 1.37E-6 based on the atmospheric isotopic ratio (Laeter et al., 2003), and R_{ter} is based on the crustal U/Th-decay (Torgersen et al., 1989).

3.3.2 Calculation method considering phase partitioning

The existence of residual DNAPL induces phase partitioning of noble gases within the groundwater. However, the location of residual DNAPL is unknown, where it may be situated from near the recharge point to near the sampling point (Fig. 3-2). Regardless of the location of residual DNAPL, the $^3He_{eq}$, $^3He_{ex}$, $^3He_{ter}$ concentration are influenced by phase partitioning. Whereas, for the $^3He_{tri}$ concentration, which is produced along the pathway of the groundwater flow after recharge, the portion of its concentration which is affected by phase partitioning varies depending on the location of residual DNAPL. Before the interaction with DNAPL, $^3He_{tri}$ is produced by the radioactive decay of ^3H. Once the groundwater comes in contact with the residual DNAPL, a portion of the previously produced $^3He_{tri}$ and recharged ^3He is partitioned to the DNAPL phase. Thereafter, along with the remaining ^3He within the groundwater, additional $^3He_{tri}$ is continuously produced by the radioactive decay of ^3H.

Based on the concepts above, the ^3H-^3He age calculation equations, which consider the influence of phase partitioning due to the existence of DNAPL along the groundwater flow path, can be modified as

$$^3He_m = (\ ^3He_{eq} + \ ^3He_{ex} + \ ^3He_{ter} + p \times \ ^3He_{tri}) \cdot F_{He} + (1-p) \times \ ^3He_{tri} \quad \text{(Eq. 3-19)}$$

where F_{He} is the degree of fractionation for He [-], which can be expressed as the fraction of ^3He left within the groundwater after phase partitioning, that

can be derived as $[i]_{water}/[i]_T$ from Eq. 3-13. p is the portion of $^3He_{tri}$ which has been phase partitioned and has a value between 0 and 1. The two end cases of 0 and 1 correspond to the situation where phase partitioning occurs near the recharge area and near the sampling area respectively.

These equations can also be rewritten as the following equations, derived by combining Eq. 3-18 and 3-19. When combining the equations together an additional term has to be considered: phase partitioning of the measured values of He and Ne. When deriving $^3He_{tri}$ from Eq. 3-18, measured values of ^{4}He and Ne are used. However, if phase partitioning is considered to have altered the ^{3}He concentration, it can be assumed that the same condition is applied for the other noble gas species as well. Hence, in order to take this into account, the degree of phase partitioning for He (F_{He}) and Ne (F_{Ne}) were divided for ^4He_m and Ne_m respectively.

$$
\begin{aligned}
{}^3He_m = \big[& R_{eq} \cdot {}^4He_{eq} + R_{ex} \cdot L_{ex} \cdot \left(Ne_m/F_{Ne} - Ne_{eq}\right) \\
& + R_{ter} \\
& \cdot \left\{ {}^4He_m/F_{He} - {}^4He_{eq} - L_{ex} \right. \\
& \left. \cdot \left(Ne_m/F_{Ne} - Ne_{eq}\right) \right\} + p \times {}^3He_{tri} \big] \cdot F_{He} \\
& + (1-p) \times {}^3He_{tri}
\end{aligned}
\qquad \text{(Eq. 3-20)}
$$

$$
\begin{aligned}
{}^{3}He_{tri} = \big[\ & {}^{3}He_{m} \\
& - \big[R_{eq} \cdot\ {}^{4}He_{eq} + R_{ex} \cdot L_{ex} \\
& \cdot \left(Ne_{m}/F_{Ne} - Ne_{eq}\right) + R_{ter} \\
& \cdot \big\{\ {}^{4}He_{m}/F_{He} -\ {}^{4}He_{eq} - L_{ex} \\
& \cdot \left(Ne_{m}/F_{Ne} - Ne_{eq}\right)\big\}\big] \cdot F_{He}\big]/(p \times F_{He} \\
& - p + 1)
\end{aligned}
\qquad \text{(Eq. 3-21)}
$$

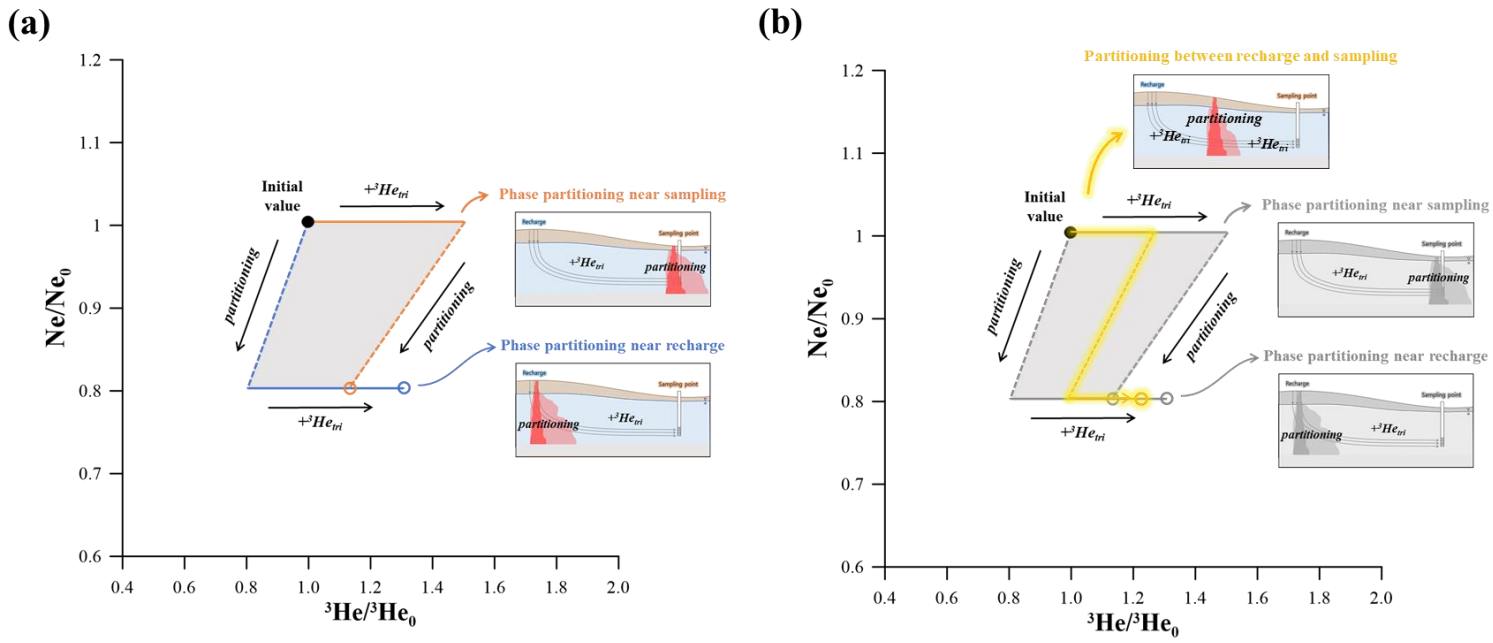

Fig. 3-2. Relative concentration changes of ^{3}He and Ne concentrations depending on the location of phase partitioning due to the existence of the DNAPL phase: (a) cases of phase partitioning near the sampling area and recharge area, (b) case of phase partitioning between the recharge and sampling area. Solid lines represent the procedure of tritiogenic helium addition due to the decay of tritium and the dotted lines represent the procedure of phase partitioning due to the existence of the DNAPL phase.

3.3.3 Age calculation cases

Groundwater age calculation was conducted for two main cases: phase partitioning not considered (PPX), phase partitioning considered (PPY). For the case of PPX, R_{ter} was varied between the determined range as mentioned in Chapter 3.2.2. In the case for PPY, the portion of $^{3}He_{tri}$ influenced by phase partitioning (p) was varied from 0 to 1, and for each case the R_{ter} was varied for the same determined range that was applied to the PPX case.

4 RESULTS AND DISCUSSION

4.1 Influence factors of the groundwater age calculation

4.1.1 Atmospheric concentration determination

The four different excess air models are capable of explaining various situations of excess air inclusion to the groundwater near the groundwater table. The best fit excess air model for each sample was determined through the program Noble90 via the process explained in Chapter 3.2.1. As a result, for the samples from September 2021, the UA and PD model showed a probability $p(\chi^2)$ larger than the threshold value of 1% for all samples (Table 4-1) (Kipfer et al., 2002). In terms of probability, the PD model is predicted to be the best fit. However, initial excess air values range between 128% to 847% which is out of the reasonable range for unconfined aquifer conditions (Kipfer et al., 2002). Hence, the application of the PD model is unrealistic, which concludes that the UA model best explains the noble gas concentrations of September 2021. In the case for the samples from April 2022, the UA model is the only model which satisfies $p(\chi^2) > 1\%$ (Table 4-2). Therefore, the UA model is determined to be the best fit excess air model for both sampling campaigns. However, NDMW-09 is not explainable by any of the excess air models for both sampling campaigns, so this well is excluded from further analysis.

In cases where more than one excess air model is concluded to be applicable, the type of model selected strongly influences the calculation of $^3He_{tri}$. For this reason, numerous studies have analyzed the impact of the choice of excess air models and evaluated its influence (Aeschbach-Hertig et al., 2008; Visser et al., 2014). However, since the UA model is the only excess

air model reasonable for the samples within this study area, groundwater age deviation due to excess air model selection can be neglected.

Table 4-1. Noble90 results of the measured noble gas concentrations during September, 2021. Samples for this sampling campaign are denoted with 'S' at the end.

	UA model				PD model			
Well	**prob [%]**	**T [°C]**	**A [ccSTP/g]**	**excess air [% Ne]**	**prob [%]**	**T [°C]**	**A [ccSTP/g]**	**excess air [% Ne]**
NDMW-09S	0.814	17.7	0.00196	18.9	64.0	9.83	0.0316	285
NDMW-10S	11.1	8.92	0.00597	53.3	81.8	5.54	0.0227	195
NDMW-11S	11.5	11.3	0.00880	80.3	71.7	8.22	0.0757	671
NDMW-12S	6.78	11.8	0.00586	55.9	78.5	8.01	0.0849	751
NDMW-13S	6.91	8.92	0.00837	74.6	64.6	6.15	0.0977	847
NDW-09S	17.3	11.2	0.00607	55.3	31.6	8.92	0.0144	129

Table 4-2. Noble90 results of the measured noble gas concentrations during April, 2022. Samples for this sampling campaign are denoted with 'A' at the end.

	UA model			
Well	**prob [%]**	**T [°C]**	**A [ccSTP/g]**	**excess air [% Ne]**
BH-1A	5.87	9.31	0.00101	9.05
MW-2A	1.79	9.98	0.00509	45.9
MW-4A	9.82	9.88	0.00834	75.0
NDMW-09A	0.00	78.60	0.00167	24.1
NDMW-11A	11.11	10.87	0.00949	86.2
NDMW-12A	8.58	7.11	0.00351	30.7
NDMW-13A	2.59	6.79	0.00703	61.4

4.1.2 Terrigenic source determination

During the calculation procedure of ^{3}H-^{3}He age, the terrigenic source of helium which is taken into account by the term R_{ter} can lead variation to the age calculation. This is due to the uncertainty of the value for this study site due to the lack of knowledge about the terrigenic source. Hence, in this study, a range for the value R_{ter} was defined to evaluate the influence of the value variation on the age calculation. The minimum value was defined as 0 which indicates no terrigenic source, and the maximum value was interpreted based the measured $^{3}He/^{4}He$ ratio and Ne/He ratio described in Fig. 4-1. All sample points obtained during the two sampling campaigns were plotted. A regression line of these sample points was obtained which was expressed as $y = 3.05\text{E} - 07\text{x} + 1.58\text{E} - 7$. The R^2 value for the regression line was determined to be 0.91 which indicates a good representation of the sample points. The y-intercept value is interpreted as the terrigenic $^{3}He/^{4}He$ ratio under the assumption that the atmospheric and tritiogenic origin is negligible at this point. Hence, the maximum R_{ter} value was interpreted to be 1.58E-7.

To determine the relative influence of the terrigenic source among the samples, excess air corrected helium values were analyzed (Fig. 4-2). Analysis of the helium concentrations excluding the excess origin in comparison to the equilibrium value allowed to distinguish between non-atmospheric factors that alter the helium concentration. These factors include the following: (1) addition of He from the terrigenic source, (2) addition of He from the tritiogenic production, (3) additional deviation of He due to physical processes. Fig. 4-2 shows that NDMW-12 is strongly influenced by the terrigenic source followed up by NDMW-10 and NDW-09. This kind of trend for NDMW-12 is consistent for both sampling campaigns, showing high persistency of the terrigenic source and relatively low influence by the other helium sources. As for the majority of other wells, they all showed relatively

high influence of tritiogenic helium or alteration due to physical processes (i.e., phase partitioning).

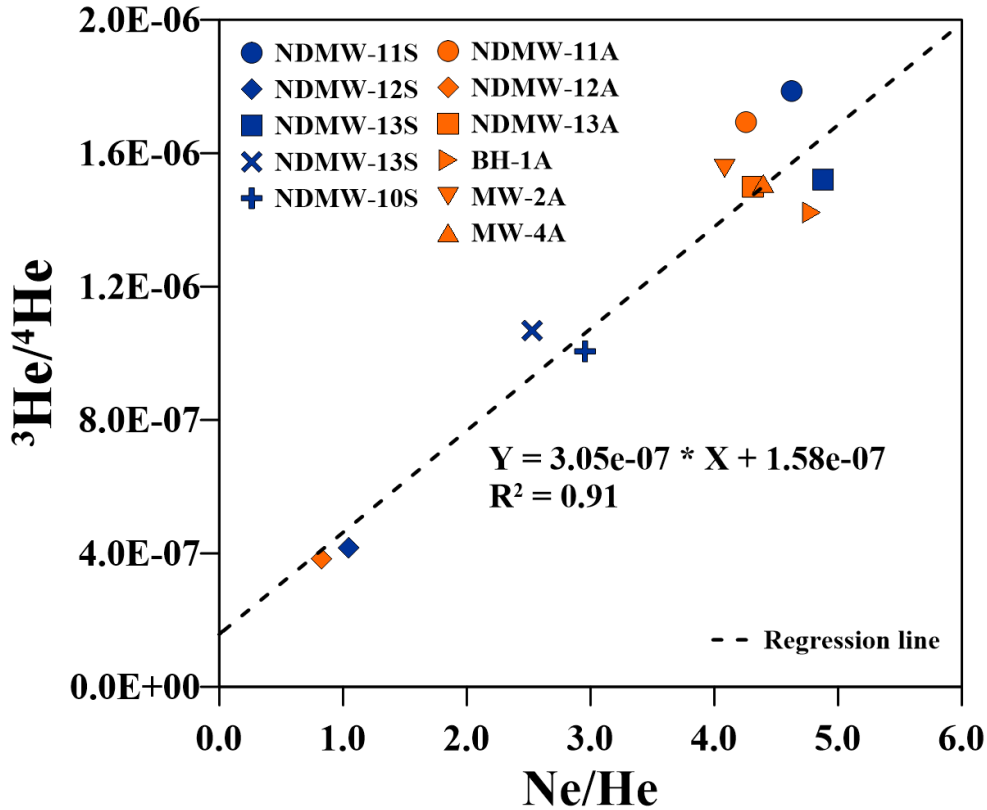

Fig. 4-1. Estimation of maximum R_{ter} (terrigenic $^3He/^4He$) value using the measured $^3He/^4He$ ratio and measured ratio between Ne and He.

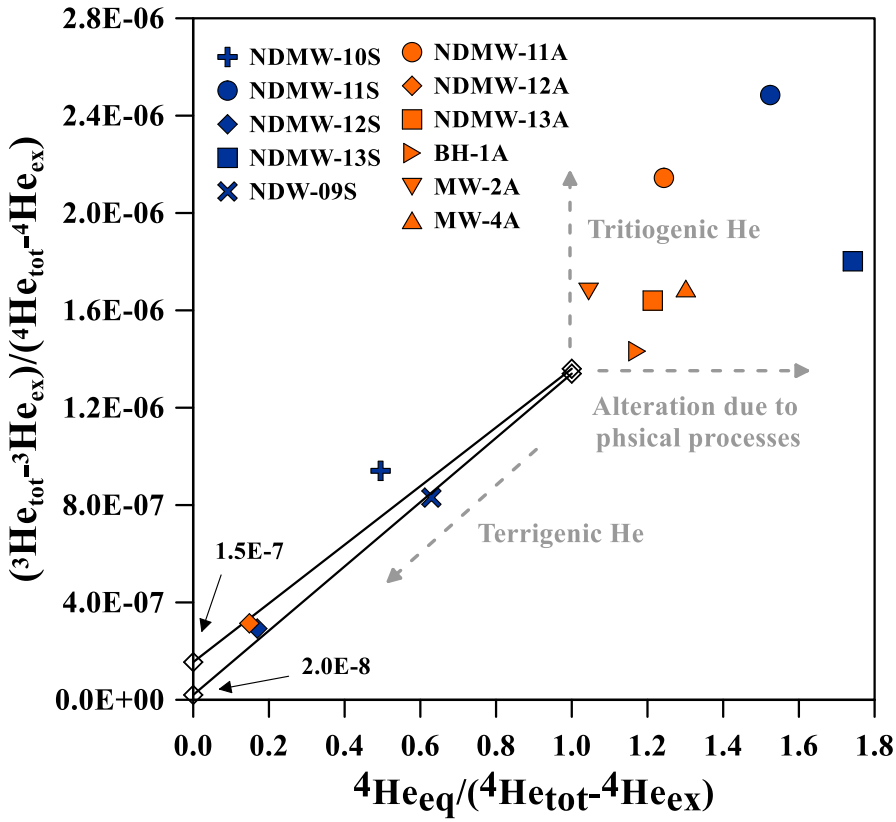

Fig. 4-2. Excess air corrected helium origin analysis: Helium source identification of groundwater samples based on ASW (12℃), terrigenic He (*: based on samples; **: typical value), tritiogenic He.

4.1.3 Phase partitioning between DNAPL and water

In order to determine the influence of phase partitioning to the ^{3}H-^{3}He groundwater age, the degree of noble gas phase partitioning for each sample was determined based on Eq. 3-13. Among the atmospheric noble gases, ^{20}Ne and ^{36}Ar were used for analysis (Fig. 4-3). Based on the derived recharge temperature and excess air model in Chapter 4.1.1, the air saturated water (ASW) and excess air relationship between ^{20}Ne and ^{36}Ar could be analyzed as the star and grey black line respectively in Fig. 4-3. The relative amount of DNAPL contacted along the flow path of the sample (V_{DNAPL}/V_{water}) was determined based on the extent of deviation from the excess air line (solid grey line). The determined values ranged from near 0 to 0.05 for the samples of September 2021, and from 0.05 to 0.08 for the samples of April 2022. For each sampling campaign, NDMW-11 was derived to have the highest value which was followed up by NDMW-13. Based on the wells that were sampled for both sampling campaigns (NDMW-11, NDMW-12, NDMW-13), the values for April 2022 showed higher values than September 2021, indicating an increase in phase partitioning experienced by the samples.

With the determined V_{water}/V_{DNAPL} value for each sample, the degree of phase partitioning for He and Ne were calculated from Eq. 3-13 (Table 4-3). Values for F_{Ne} were between 0.882–0.983, and F_{He} varied between 0.841–0.997. These values indicate that depending on the degree of phase partitioning, noble gas concentrations can be influenced from as small as 0.3% to as large as 16.9%.

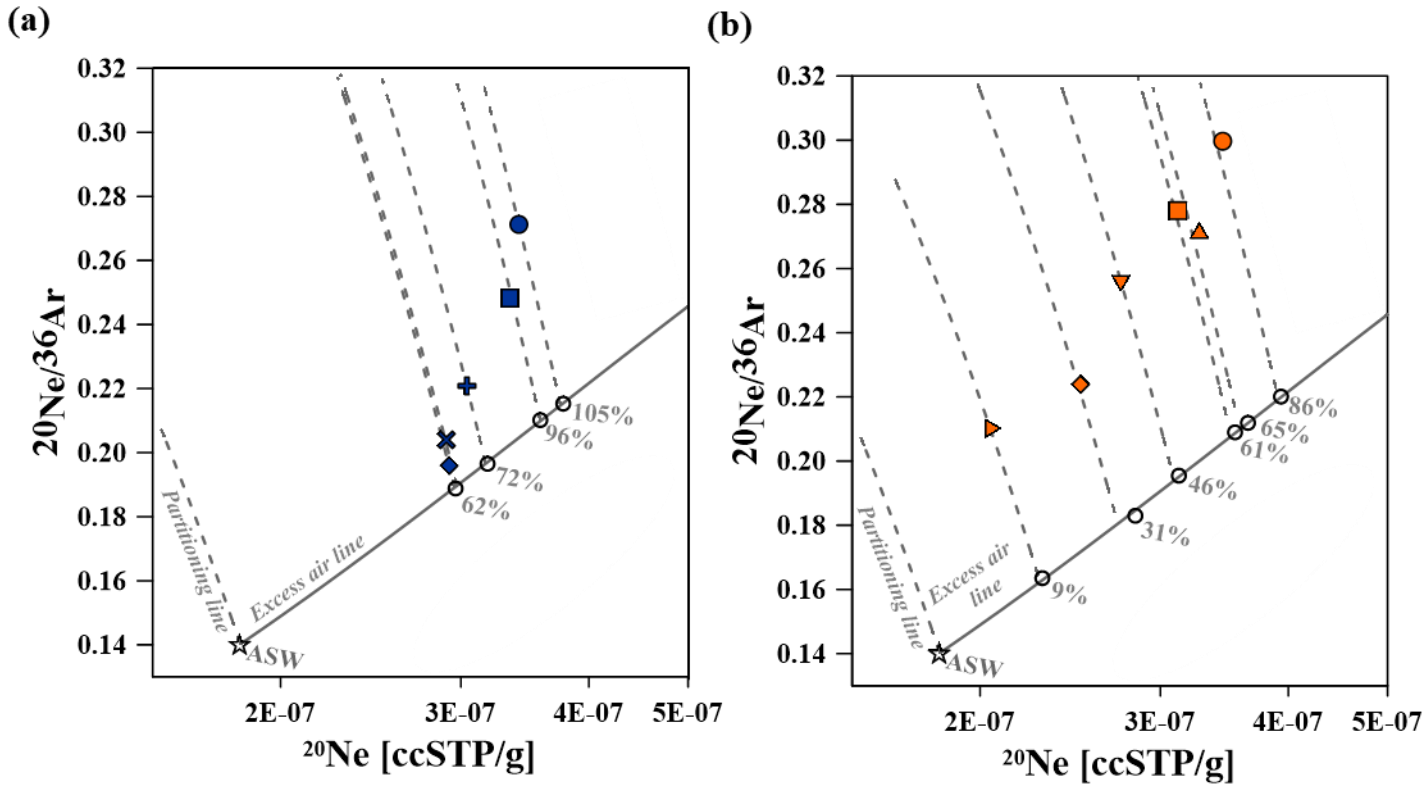

Fig. 4-3. Analysis of the degree of phase partitioning based on the relationship between ^{20}Ne and ^{36}Ar: (a) September 2021, (b) April 2022.

Table 4-3. Calculated values of V_{DNAPL}/V_{water}, F_{Ne}, F_{He} for each well of the two sampling campaigns (September 2021, April 2022).

Well	V_{DNAPL}/V_{water}	F_{Ne}	F_{He}
NDMW-10S	0.02	0.968	0.955
NDMW-11S	0.05	0.923	0.894
NDMW-12S	0.01	0.983	0.977
NDMW-13S	0.04	0.937	0.914
BH-1A	0.07	0.895	0.858
MW-2A	0.07	0.895	0.858
MW-4A	0.06	0.908	0.876
NDMW-11A	0.08	0.882	0.841
NDMW-12A	0.05	0.923	0.894
NDMW-13A	0.07	0.895	0.858

4.2 Groundwater age calculation for each case

4.2.1 Groundwater age calculation with no phase partitioning considered

Groundwater age calculation was conducted for varying R_{ter} values. Calculation results for the cases of no terrigenic source ($R_{ter} = 0$), typical value of terrigenic source (R_{ter} = 2E-08; Mamyrin and Tolstikhin, 1984), and the estimated maximum value of terrigenic source (R_{ter} =1.5E-7) are shown in Table 4-4.

Based on Eqs. 3-14 and 3-18, the relationship between the R_{ter} value and ^{3}H-^{3}He age can be derived, where an increase in R_{ter} resulted in a decrease in $^{3}He_{tri}$ which consequently decreases the age calculated. In other words, as R_{ter} increased, the calculated ^{3}H-^{3}He age decreased.

This characteristic was identified for samples NDMW-10S, NDMW-12S, NDW-09S, MW-2A, NDMW-11A, NDMW-12A, and NDMW-13A where age was calculated to decrease with increasing R_{ter} (Fig. 4-4). It corresponds to the pattern identified by Mahara et al.(2014) where the neglection of the terrigenic source ($R_{ter} = 0$) was evaluated to overestimate the groundwater age. Among these samples, NDMW-12S and NDMW-12A showed the largest changes in age due to the varying R_{ter} values which were followed up by NDMW-10S and NDW-09S. This is correlated to the fact that NDMW-12S, NDMW-12A, NDMW-10S, and NDW-09S were analyzed to be highly influenced by the terrigenic source as described in Chapter 4.1.2 (Fig. 4-2). The calculated terrigenic ^{4}He ($^{4}He_{ter}$) values for these samples had the four highest values (Table 4-5). Due to the high $^{4}He_{ter}$ concentrations, the variation of R_{ter} had relatively large impact on the age calculation to these samples compared to the samples of low $^{4}He_{ter}$ concentrations (Eq. 3-18). Hence, the groundwater age influencing factor of R_{ter} had a large impact in the case of samples highly influenced by the terrigenic source.

The maximum age difference due to the variation of R_{ter} was highest for NDMW-12S and NDMW-12A which were 43.6 yrs and 30 yrs respectively. The other samples depicted a maximum age difference up to 6.7 years.

Unlike the samples mentioned above, there were samples (NDMW-11S, NDMW-13S, BH-1A, MW-4A) that showed an opposite trend to the predicted, where the groundwater age increased with the increase of R_{ter}. This was due to the negative $^4He_{ter}$ concentration calculated (Table 4-5). The possible reasons for the negative value can be interpreted in terms of two aspects: (1) overestimation of excess air concentration, (2) exclusion of noble gas phase partitioning to the DNAPL phase. In the study of noble gases which use the excess air models to determine the terrigenic concentration ($^4He_{ter}=^4He_m-^4He_{eq}-^4He_{ex}$), there are many cases where the $^4He_{ter}$ is calculated to be negative (Shapiro et al., 1999; Kipfer et al., 2002; Visser et al., 2014). In the case of Visser et al. (2014), the negative values of $^4He_{ter}$ were predicted to be due to excessive fractionation of excess air, larger than that can be calculated by the fitted excess air models. Kipfer et al. (2002) showed that the assumption of $L_{ex}=L_{air}=0.288$ was the reason for the negative values and suggested varying values of L_{ex} depending on the excess air model applied and the degree of excess air fractionation determined. While both of these studies focus on the excess air overestimation, Mahara et al. (2014) suggested that degassing had influenced the measured concentration which resulted a calculation of negative terrigenic concentration for some samples. These studies indicated that phase partitioning of noble gases to DNAPL could potentially be a reason for the calculation of negative values. Hence, the verification of the reason for these negative terrigenic values are determined in Chapter 4.2.2 where phase partitioning is considered in age calculation.

Table 4-4. ^{3}He-^{3}He age calculation for cases of no terrigenic source (R_{ter} = 0), typical value of terrigenic source (R_{ter} = 2E-8), and the estimated maximum value of terrigenic source (R_{ter} = 1.5E-7).

Well	R_{ter}=0	R_{ter}=2E-8	R_{ter}=1.5E-7
NDMW-10S	39.1	38.6	35.1
NDMW-11S	26.1	26.2	26.6
NDMW-12S	28.2	25.7	-81.9
NDMW-13S	-1.6	-1.1	1.85
NDW-09S	14.9	14.1	8.22
BH-1A	0.7	0.7	0.7
MW-2A	36.6	36.5	35.9
MW-4A	18.7	18.8	18.9
NDMW-11A	35.3	35.3	35.2
NDMW-12A	28.7	26.9	6.7
NDMW-13A	19.4	19.4	19.1

Table 4-5. Calculated $^{4}He_{ter}$ value for each well sampled at September 2021 and April 2022.

Well	$^{4}He_{ter}$
NDMW-10S	5.69E-08
NDMW-11S	-6.37E-09
NDMW-12S	2.35E-07
NDMW-13S	-8.75E-09
NDW-09S	3.59E-08
BH-1A	-3.78E-10
MW-2A	6.19E-09
MW-4A	-1.14E-09
NDMW-11A	7.31E-10
NDMW-12A	2.73E-07
NDMW-13A	2.24E-09

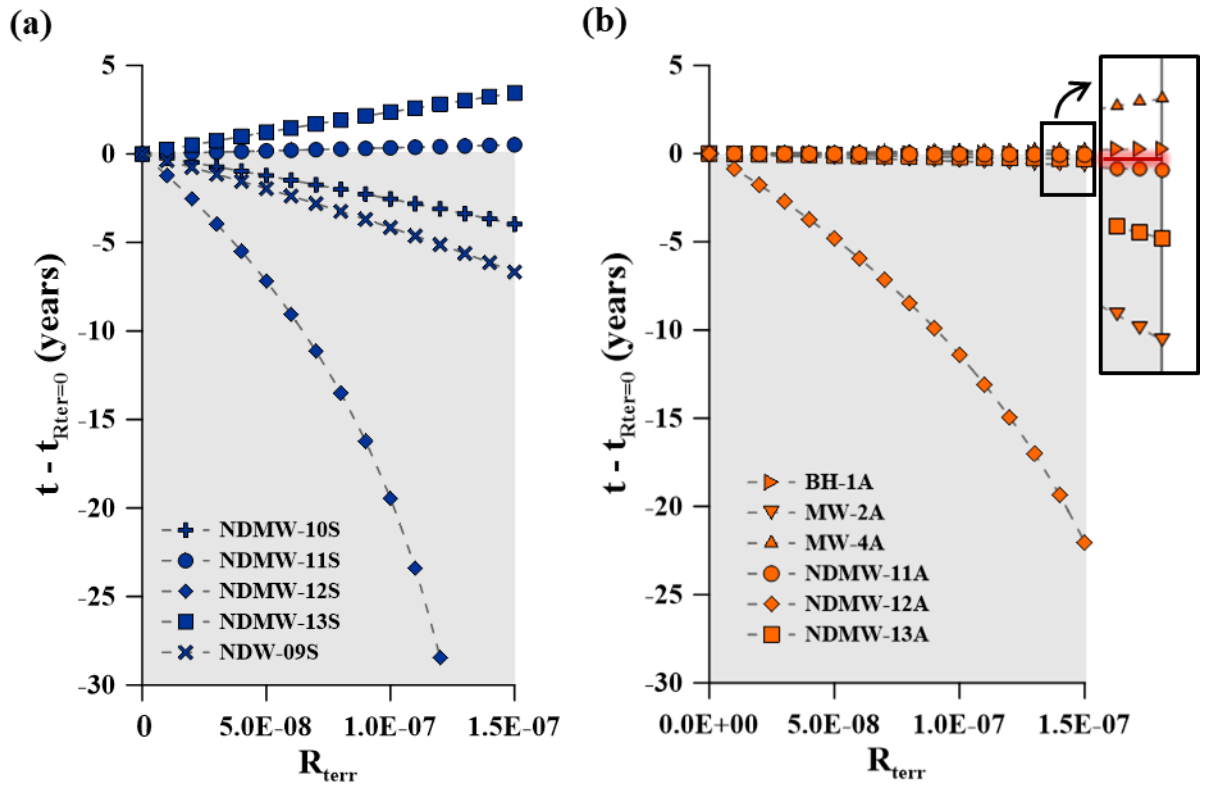

Fig. 4-4. Age variation from the age calculated for the case of no terrigenic source (t-$t_{Rter=0}$) for each sample with varying R_{ter} values. Grey area indicates the area of negative t-$t_{Rter=0}$ values.

4.2.2 Groundwater age calculation with phase partitioning considered

Noble gas phase partitioning to DNAPL was analyzed for samples as described in Chapter 4.1.3. The influence of this factor was analyzed based on the derived equations which are expressed as Eq. 3-14 and 3-21. Based on these equations, the influence of the consideration of phase partitioning and the influence of the varying portion of ^{3}He affected by the phase partitioning were evaluated.

When considering phase partitioning, all samples resulted a decrease in age with increasing R_{ter}, except for NDMW-11S and NDMW-13S (Fig. 4-5). By comparing this with the results of the case of no phase partitioning considered in Chapter 4.2.1, for BH-1A and MW-4A the consideration of phase partitioning provided calculations of positive $^{4}He_{ter}$ concentrations. This led to age calculations that followed the predicted trend of decreasing age with increasing R_{ter} values (Table 4-6). As for NDMW-11S and NDMW-13S, their consistent calculation of negative $^{4}He_{ter}$ values indicated that they cannot be fully explained by the influence of phase partitioning and additional influencing factors have to be considered. Hence, age analysis for these two samples were neglected for further analysis.

The consideration of phase partitioning resulted an increase in calculated groundwater age for all samples (Fig. 4-6). This is due to the fact that considering phase partitioning allowed to derive the corrected noble gas concentration for the time of recharge which is higher than the concentration at the sampling point. The degree of increase varied for each sample, and was analyzed by the mean difference between the calculated age of varying p values and the calculated age of no phase partitioning, while R_{ter} was fixed to the typical value of 2.0E-8. The smallest age difference due to phase partitioning was depicted by NDMW-12S (0.4 years) and the largest was

shown by MW-4A (3.6 years). The age difference due to the consideration of phase partitioning was positively correlated to the estimated volume ratio between DNAPL and water for the corresponding sample (Fig 4-7). This indicated that the larger the estimated DNAPL to have been contacted by the water sample along the flow path, the more phase partitioning the sample had experienced, which deviated the age calculation to a larger extent.

The portion of $^{3}He_{tri}$ that was phase partitioned (p) also varied the groundwater age. As the value of p increased, which corresponds to the situation where the location of phase partitioning due to DNAPL gets closer to the sampling point, the calculated age also increased (Fig. 4-6). The variation of age due to the p value has a positive correlation with the average groundwater age (Fig 4-8).

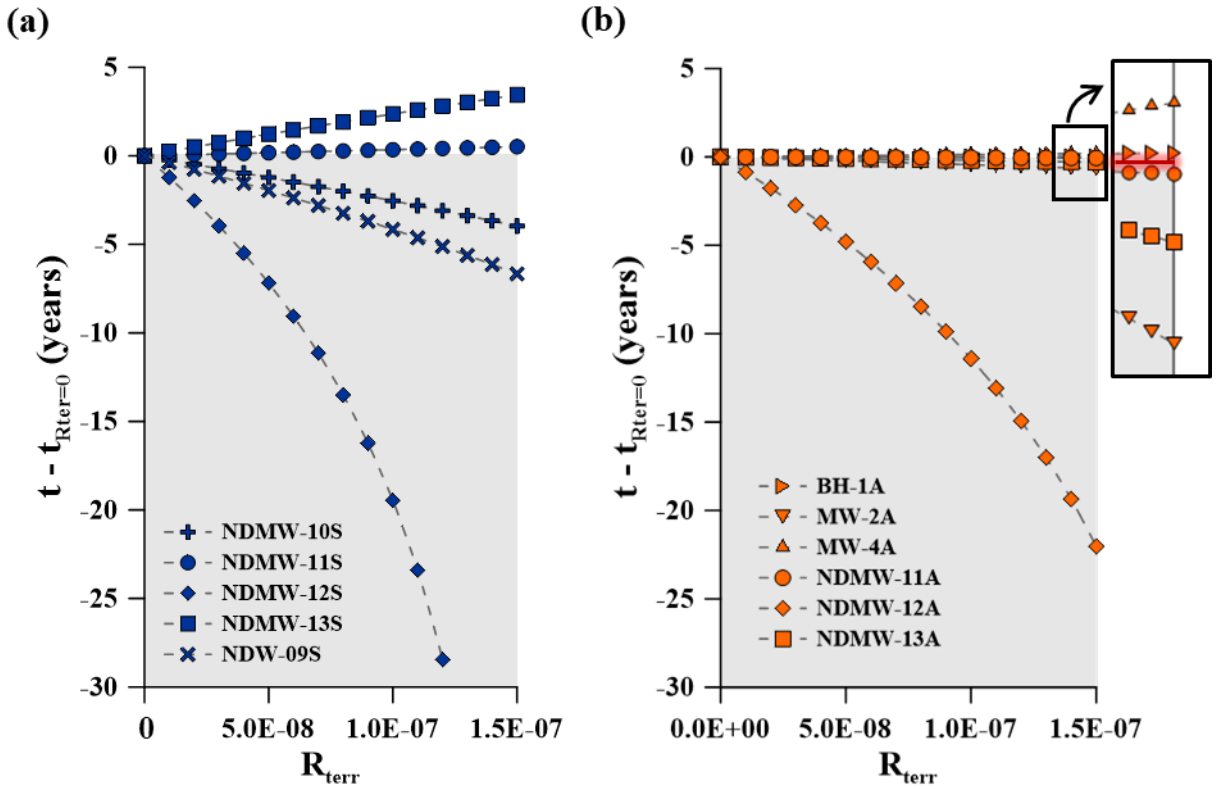

Fig. 4-5. Age variation from the age calculated for the case of no terrigenic source (t-$t_{Rter=0}$) for each sample when phase partitioning of noble gases is considered with varying R_{ter} values. Grey area indicates the area of negative t-t$_{Rter=0}$ values.

Table 4-6. Calculated $^{4}He_{ter}$ value after considering phase partitioning of noble gases for each well sampled at September 2021 and April 2022.

Well	$^{4}He_{ter}$
NDMW-10S	6.02E-08
NDMW-11S	-5.06E-09
NDMW-12S	2.40E-07
NDMW-13S	-8.07E-09
NDW-09S	3.59E-08
BH-1A	4.38E-10
MW-2A	9.09E-09
MW-4A	9.27E-10
NDMW-11A	4.17E-09
NDMW-12A	3.06E-07
NDMW-13A	4.79E-09

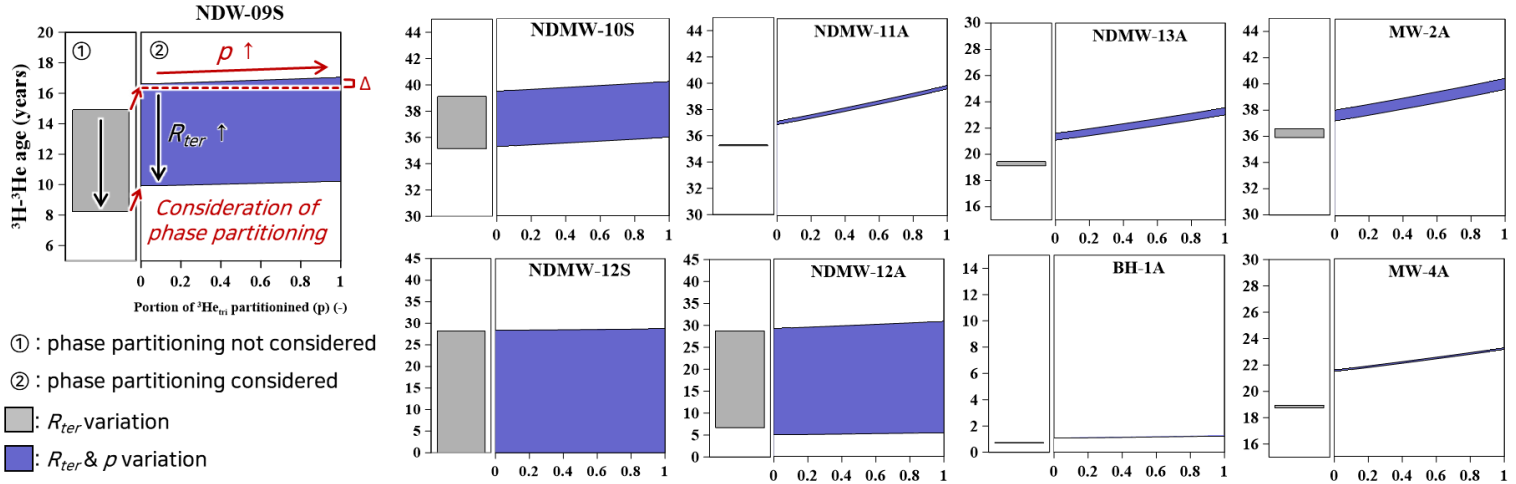

Fig. 4-6. Groundwater age calculation trends when phase partitioning is not considered (grey) and is considered (purple). When phase partitioning of noble gases is considered, the value of R_{ter} and p are varied.

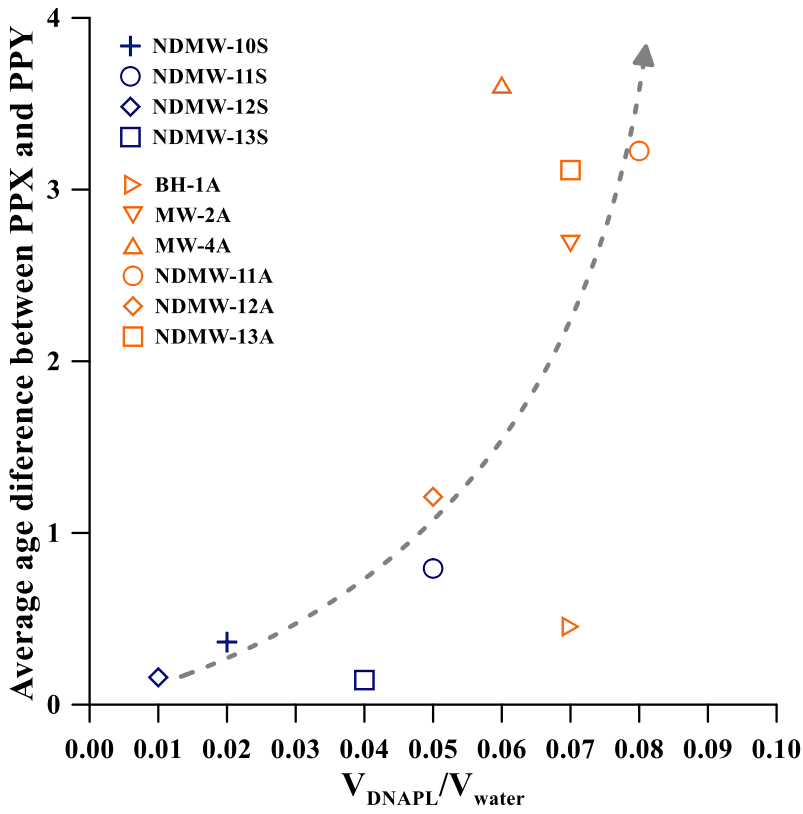

Fig. 4-7. Comparison between V_{DNAPL}/V_{water} and the average age difference between cases of no phase partitioning consideration (PPX) and with phase partitioning consideration (PPY). The dotted line indicates the trend of relationship between the two variables, which indicate a positive relationship.

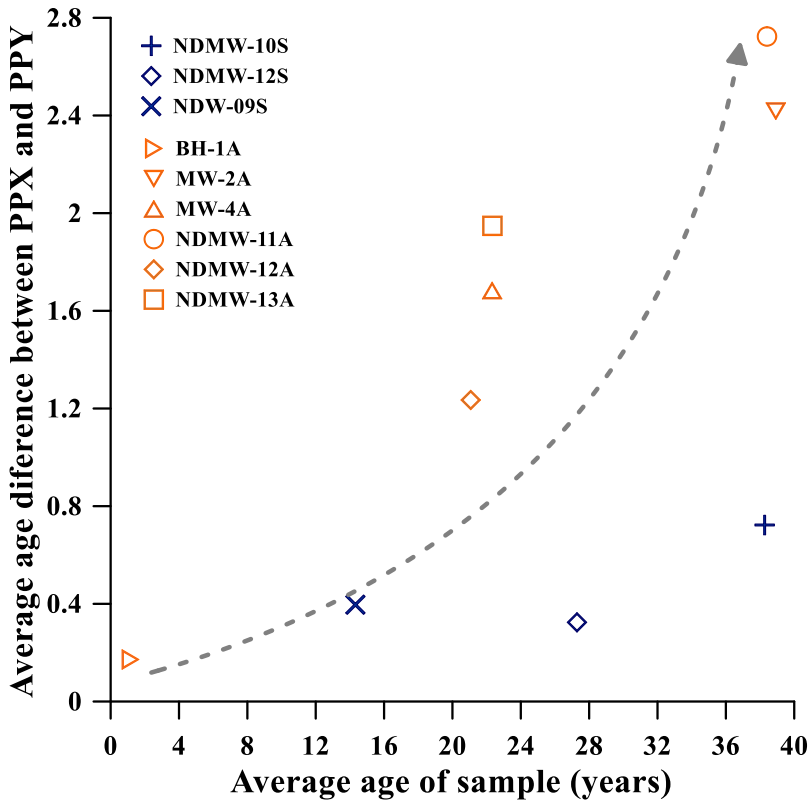

Fig. 4-8. Comparison between the average age of the sample and the average age difference between cases of no phase partitioning consideration (PPX) and with phase partitioning consideration (PPY). The dotted line indicates the trend of relationship between the two variables, which indicate a positive relationship.

4.3 Groundwater age variations due to influence factors

Evaluation of the groundwater age variation due to phase partitioning was conducted in comparison with other influencing factors for the determination of its significance. The initial intention was to consider age differences due to atmospheric concentration determination, terrigenic source determination, and phase partitioning. However, as the atmospheric concentration was only explainable with one excess air model, which was the UA model, only two influencing factors (terrigenic source, phase partitioning) were compared. As the base model of comparison, the case of no phase partitioning with a R_{ter} value of 2.0E-8 (typical value) was used.

As a result, for the case of no phase partitioning considered, groundwater age variation from the base case was significantly high for samples that were highly influenced by the terrigenic source (NDMW-12S, NDMW-12A, NDMW-10S, NDW-09S). Especially for NDMW-12, calculated age was differed up to 25 years due to R_{ter} variation. For the remainder samples which are relatively less influenced by the terrigenic source (BH-1A, MW-2A, MW-4A, NDMW-11A, NDMW-13A), age variations were all below 1 year (Fig. 4-9).

The overall influence of phase partitioning to the groundwater age calculation was evaluated in comparison to the base case as well. The consideration of phase partitioning itself consistently increased the age calculated, whereas the age calculation deviation due to the varying portion of $^{3}He_{tri}$ phase partitioned differed between samples. The overall influence of phase partitioning to groundwater age calculation considering these two aspects could be divided into cases of high and low influence of terrigenic source, where when terrigenic influence was low the age deviation due to phase partitioning was calculated to be relatively high (Fig. 4-9). Age

deviation from the base case was as small as 0.2 years (NDMW-12S) and as large as 4.6 years (NDMW-11A) (Table 4-7).

By comparing the degree of age calculation differences due to each influencing factor, it was shown that for the samples highly influenced by the terrigenic source, the age variation was larger due to the R_{ter} value than for phase partitioning. Whereas for cases where the terrigenic source was not significant, the consideration of phase partitioning and the variation of the timing of phase partitioning along the groundwater pathway was the dominating factor of age variation. Groundwater age variations were all above 3 years except for BH-1A. In the case for BH-1A, there were signs of deviation from the overall characteristic of the study area based on the fact that it had an exceptionally high tritium value of 19 TU.

Previous studies dealing with age calculation error showed various deviations of ages due to the influencing factors of interest. For groundwater age calculation based on various excess air models, there were cases where the calculated age differed up to 10 years (Visser et al., 2014; Peeters et al., 2003). Degassing was also considered in terms of groundwater age calculation when using the ^{3}H-^{3}He age tracer and was evaluated to have an average of 3 years effect on groundwater age calculation (Visser et al., 2007). There is no absolute number to which groundwater age deviation is termed significantly large. However, these studies have pointed out in common that the consideration of the variation due to the possible factors within the study area of interest is important. Being informed of the proper age calculation error provides further insight during the application of this calculated age. An example is the calculation of groundwater velocity with the use of groundwater age (Kaown et al., 2014). With a more complete understanding of the error of the calculated groundwater age, misleading interpretations of the possible range of groundwater velocities can be prevented.

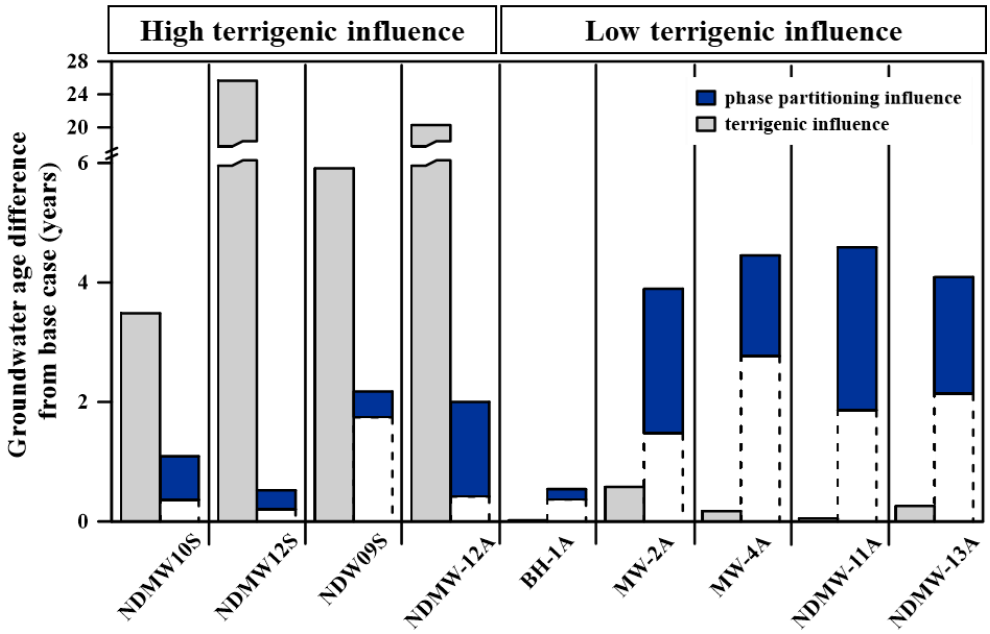

Fig. 4-9. Groundwater age variation due to influencing factors: terrigenic influence (grey bar), phase partitioning influence (blue bar).

Table 4-7 Age deviation from the base case (no phase partitioning, R_{ter}=2.0E-8) for each influencing factor.

Well	Terrigenic influence	Phase partitioning influence
NDMW-10S	3.5	1.1
NDMW-12S	25.7	0.5
NDW-09S	5.9	2.2
BH-1A	0.1	0.5
MW-2A	0.6	3.9
MW-4A	0.2	4.5
NDMW-11A	0.1	4.6
NDMW-12A	20.3	2.0
NDMW-13A	0.3	4.1

5 CONCLUSION

In this study, the influence of phase partitioning to DNAPL on the ^{3}H-^{3}He age calculation was analyzed in comparison to other influencing factors. The influencing factors of atmospheric concentration determination and terrigenic source determination were used to compare its influence on groundwater age calculation to the influence induced by phase partitioning. Atmospheric concentration determination impact was evaluated by determining the possible excess air models applicable for the samples in the study area. For this study, the UA model was the only excess air model applicable, so the variation of groundwater age due to the selection of excess air model was neglected. As for the terrigenic source determination, the possible range of values for the related parameter of R_{ter} was defined, which was determined to be between 0 and 1.5E-7. Last of all, the degree of phase partitioning each sample had gone through was evaluated based on the noble gas concentrations for each sample. In order to take this phase partitioning characteristic into account, a modified equation to determine the influence of phase partitioning itself and the portion of $^{3}He_{tri}$ influenced was proposed. Based on these determined ranges for each influence factor, the groundwater age variation was determined for each factor and the impact by phase partitioning was evaluated. It was determined that samples evaluated to have low terrigenic source impact were highly influenced by phase partitioning, which resulted up to 4.6 years of variation. The perception of the range of error that can be induced by noble gas phase partitioning at a DNAPL contaminated site provides further insight during the application of the calculated groundwater age. Hence, the consideration of site specific influencing factors to the ^{3}H-^{3}He age calculation is essential.

6 REFERENCE

Aeppli, C., Hofstetter, T. B., Amaral, H. I., Kipfer, R., Schwarzenbach, R. P., & Berg, M. (2010). Quantifying in situ transformation rates of chlorinated ethenes by combining compound-specific stable isotope analysis, groundwater dating, and carbon isotope mass balances. *Environmental Science & Technology*, *44*(10), 3705-3711.

Aeschbach-Hertig, W., Peeters, F., Beyerle, U., & Kipfer, R. (2000). Palaeotemperature reconstruction from noble gases in ground water taking into account equilibration with entrapped air. *Nature*, *405*(6790), 1040-1044.

Aeschbach-Hertig, W., Peeters, F., Beyerle, U., & Kipfer, R. (1999). Interpretation of dissolved atmospheric noble gases in natural waters. *Water Resources Research*, *35*(9), 2779-2792.

Aeschbach-Hertig, W., & Solomon, D. K. (2013). Noble gas thermometry in groundwater hydrology. *The noble gases as geochemical tracers*, 81-122.

Andrews, J. N., & Lee, D. J. (1979). Inert gases in groundwater from the Bunter Sandstone of England as indicators of age and palaeoclimatic trends. *Journal of Hydrology*, *41*(3-4), 233-252.

Ballentine, C. J., Burgess, R., & Marty, B. (2002). Tracing fluid origin, transport and interaction in the crust.

Bouchard, D., Enfield, C., & Piwoni, M. (1989). Transport processes involving organic chemicals. *Reactions and movement of organic chemicals in soils*, *22*, 349-371.

Brusseau, M. L. (1992). Rate-limited mass transfer and transport of organic solutes in porous media that contain immobile immiscible organic liquid. *Water Resources Research*, *28*(1), 33-45.

Brusseau, M. L., Nelson, N. T., & Costanza-Robinson, M. S. (2003). Partitioning tracer tests for characterizing immiscible-fluid

saturations and interfacial areas in the vadose zone. *Vadose Zone Journal*, *2*(2), 138-147.

Cho, I. (2020). *Characterization of a DNAPL Contaminated Site by Partitioning Behavior of Noble Gas* Seoul National Univeristy Graduate School].

De Laeter, J. R., Böhlke, J. K., De Bievre, P., Hidaka, H., Peiser, H., Rosman, K., & Taylor, P. (2003). Atomic weights of the elements. Review 2000 (IUPAC Technical Report). *Pure and applied chemistry*, *75*(6), 683-800.

Divine, C. E., Sanford, W. E., & McCray, J. E. (2003). Helium and neon groundwater tracers to measure residual DNAPL. *Vadose Zone Journal*, *2*(3), 382-388.

Famiglietti, J. S. (2014). The global groundwater crisis. *Nature Climate Change*, *4*(11), 945-948.

Inchoen Metropolitan City Museum (2020). Namdong Industrial District: Inchoen Metropolitan City Museum academic research report (report No. 33). Incheon Metropolitan City Museum. https://www.incheon.go.kr/museum/MU010501/2061107

Kaown, D., Koh, D.-C., & Lee, K.-K. (2009). Effects of groundwater residence time and recharge rate on nitrate contamination deduced from δ18O, δD, 3H/3He and CFCs in a small agricultural area in Chuncheon, Korea. *Journal of Hydrology*, *366*(1-4), 101-111.

Kaown, D., Koh, D.-C., Solomon, D. K., Yoon, Y.-Y., Yang, J., & Lee, K.-K. (2014). Delineation of recharge patterns and contaminant transport using 3H–3He in a shallow aquifer contaminated by chlorinated solvents in South Korea. *Hydrogeology Journal*, *22*(5), 1041-1054.

Kharaka, Y. K., & Specht, D. J. (1988). The solubility of noble gases in crude oil at 25–100 C. *Applied Geochemistry*, *3*(2), 137-144.

Kipfer, R., Aeschbach-Hertig, W., Peeters, F., & Stute, M. (2002). Noble gases in lakes and ground waters. *Reviews in Mineralogy and Geochemistry*, *47*(1), 615-700.

Korea Institute of Nuclear Safety (KINS) (2011) Environmental radioactivity survey data in Korea, vol. 43, Korea Institue of Nuclear Safety, Daejon, pp 71. https://doi.org/10.23000/TRKO201300021819 (korean)

Korea Institute of Nuclear Safety (KINS) (2016) Environmental radioactivity survey data in Korea, vol. 48, Korea Institue of Nuclear Safety, Daejon, pp 73. https://clean.kins.re.kr/info/in03_rept_list.jsp (korean)

Korea Institute of Nuclear Safety (KINS) (2020) Environmental radioactivity survey data in Korea, vol. 52, Korea Institue of Nuclear Safety, Daejon, pp 64. https://clean.kins.re.kr/info/in03_rept_list.jsp (korean)

Korea Environment Coroporation (2020). Sruvey and evaluation of area where groundwater pollution is of concern in 2020: field work reocrd. (Gojan-dong, Namdong-gu, Inchoen). Korea Environment Corporation

Korean Meteorological Administration (KMA) (2022). Home page: https://data.kma.go.kr/cmmn/main.do

Lippmann, J., Stute, M., Torgersen, T., Moser, D., Hall, J., Lin, L., Borcsik, M., Bellamy, R., & Onstott, T. C. (2003). Dating ultra-deep mine waters with noble gases and 36Cl, Witwatersrand Basin, South Africa. *Geochimica et Cosmochimica Acta*, *67*(23), 4597-4619.

Lucas, L. L., & Unterweger, M. P. (2000). Comprehensive review and critical evaluation of the half-life of tritium. *Journal of Research of the National Institute of Standards and Technology*, *105*(4), 541.

Mahara, Y., Ohta, T., Morikawa, N., Nakano, T., Tokumasu, M., Hukutani, S., Tokunaga, T., & Igarashi, T. (2014). Effects of terrigenic He

components on tritium–helium dating: A case study of shallow groundwater in the Saijo Basin. *Applied Geochemistry*, *50*, 142-149.

Mamyrin BA, Tolstikhin IN (1984) Helium isotopes in nature. Elsevier, Amsterdam, 273.

Manning, A. H., Kip Solomon, D., & Thiros, S. A. (2005). 3H/3He age data in assessing the susceptibility of wells to contamination. *Groundwater*, *43*(3), 353-367.

Mihajlov, I., Mozumder, M. R. H., Bostick, B. C., Stute, M., Mailloux, B. J., Knappett, P. S., Choudhury, I., Ahmed, K. M., Schlosser, P., & van Geen, A. (2020). Arsenic contamination of Bangladesh aquifers exacerbated by clay layers. *Nature communications*, *11*(1), 1-9.

Moeck, C., Popp, A. L., Brennwald, M. S., Kipfer, R., & Schirmer, M. (2021). Combined method of 3H/3He apparent age and on-site helium analysis to identify groundwater flow processes and transport of perchloroethylene (PCE) in an urban area. *Journal of Contaminant Hydrology*, *238*, 103773.

Moeck, C., Popp, A. L., Brennwald, M. S., Kipfer, R., & Schirmer, M. (2021). Combined method of 3H/3He apparent age and on-site helium analysis to identify groundwater flow processes and transport of perchloroethylene (PCE) in an urban area. *Journal of Contaminant Hydrology*, *238*, 103773.

Morgenstern, U., Daughney, C. J., Leonard, G., Gordon, D., Donath, F. M., & Reeves, R. (2015). Using groundwater age and hydrochemistry to understand sources and dynamics of nutrient contamination through the catchment into Lake Rotorua, New Zealand. *Hydrology and Earth System Sciences*, *19*(2), 803-822.

Morrison, R. D. (2000). Application of forensic techniques for age dating and source identification in environmental litigation. *Environmental forensics*, *1*(3), 131-153.

Murphy, S., Ouellon, T., Ballard, J.-M., Lefebvre, R., & Clark, I. D. (2011). Tritium–helium groundwater age used to constrain a groundwater flow model of a valley-fill aquifer contaminated with trichloroethylene (Quebec, Canada). *Hydrogeology Journal*, *19*(1), 195-207.

Peeters, F., Beyerle, U., Aeschbach-Hertig, W., Holocher, J., Brennwald, M. S., & Kipfer, R. (2003). Improving noble gas based paleoclimate reconstruction and groundwater dating using 20Ne/22Ne ratios. *Geochimica et Cosmochimica Acta*, *67*(4), 587-600.

Schmoll, O., Howard, G., Chilton, J., & Chorus, I. (2006). *Protecting groundwater for health: managing the quality of drinking-water sources*. World Health Organization.

Shapiro, S. D., LeBlanc, D., Schlosser, P., & Ludin, A. (1999). Characterizing a sewage plume using the 3H-3He dating technique. *Groundwater*, *37*(6), 861-878.

Solomon, D., Gilmore, T., Solder, J., Kimball, B., & Genereux, D. (2015). Evaluating an unconfined aquifer by analysis of age-dating tracers in stream water. *Water Resources Research*, *51*(11), 8883-8899.

Solomon, D., Poreda, R., Cook, P., & Hunt, A. (1995). Site Characterization Using 3H/3 He Ground-Water Ages, Cape Cod, MA. *Groundwater*, *33*(6), 988-996.

Solomon, D., Poreda, R., Schiff, S., & Cherry, J. (1992). Tritium and helium: 3 as groundwater age tracers in the Borden aquifer. *Water Resources Research*, *28*(3), 741-755.

Stute, M., Forster, M., Frischkorn, H., Serejo, A., Clark, J. F., Schlosser, P., Broecker, W. S., & Bonani, G. (1995). Cooling of tropical Brazil (5 C) during the last glacial maximum. *Science*, *269*(5222), 379-383.

Sültenfuβ, J., Purtschert, R., & Führböter, J. F. (2011). Age structure and recharge conditions of a coastal aquifer (northern Germany)

investigated with 39 Ar, 14 C, 3 H, He isotopes and Ne. *Hydrogeology Journal*, *19*(1), 221-236.

Tolstikhin, I. (1969). Determination of groundwater age by the T-^ 3He method. *Geochemistry International*, *6*, 810-811.

Torgersen, T. (1989). Terrestrial helium degassing fluxes and the atmospheric helium budget: Implications with respect to the degassing processes of continental crust. *Chemical Geology: Isotope Geoscience Section*, *79*(1), 1-14.

Torgersen, T., Top, Z., Clarke, W., Jenkins, W., & Broecker, W. (1977). A new method for physical limnology—tritium-helium-3 ages—results for Lakes Erie, Huron, and Ontario 1. *Limnology and Oceanography*, *22*(2), 181-193.

Unterweger, M., Coursey, B., Schima, F., & Mann, W. (1980). Preparation and calibration of the 1978 National Bureau of Standards tritiated-water standards. *The International Journal of Applied Radiation and Isotopes*, *31*(10), 611-614.

Visser, A., Broers, H. P., & Bierkens, M. F. (2007). Dating degassed groundwater with 3H/3He. *Water Resources Research*, *43*(10).

Visser, A., Fourré, E., Barbecot, F., Aquilina, L., Labasque, T., Vergnaud, V., & Esser, B. K. (2014). Intercomparison of tritium and noble gases analyses, 3H/3He ages and derived parameters excess air and recharge temperature. *Applied Geochemistry*, *50*, 130-141.

Weiss, R. (1970). The solubility of nitrogen, oxygen and argon in water and seawater. Deep Sea Research and Oceanographic Abstracts,

Weiss, R. F. (1971). Solubility of helium and neon in water and seawater. *Journal of Chemical & Engineering Data*, *16*(2), 235-241.

Weiss, R. F., & Kyser, T. K. (1978). Solubility of krypton in water and sea water. *Journal of chemical and engineering data*, *23*(1), 69-72.

국문 초록

지하수의 흐름과 오염물질의 이동을 이해하기 위한 인자로서 $^{3}H-^{3}He$ 연령추적자가 널리 사용되었다. 기존의 연령 계산 방법은 지하수 흐름과 함께 ^{3}He 농도가 보존된다는 기본적인 가정을 기반으로 하였다. 하지만 DNAPL 이 지하수 내 존재하는 상황에서 비활성기체의 DNAPL 로의 상분배 특성에 의해 이 가정은 위배 될 수 있다. 이에 연령을 계산하는 과정에서 이러한 DNAPL 로의 비활성기체 상분배가 영향 주는 정도를 평가하기 위해 연령 계산에 영향을 주는 다른 영향인자들과의 비교분석이 이루어졌다. 이를 위해 비활성기체의 DNAPL 로의 상분배를 고려할 수 있는 식을 제안하였고, 본 연구에 적용하였다. 본 연구가 이루어진 지역은 인천에 위치하고 있는 남동공단이며, 이 곳은 DNAPL 로 오염된 것으로 알려져 있다. 연구 결과, terrigenic source 에 의한 영향이 적은 것으로 판별된 관정의 경우 연령 계산 과정에서 다른 영향인자에 의한 영향보다 상분배에 의한 영향이 큰 것으로 나타났다. 상분배가 일어난 현상 자체를 고려하는 것과 상분배에 영향 받은 tritiogenic helium 의 정도에 따른 연령 계산을 한 결과 4.6 년까지 차이를 보였다. 본 연구를 통해 DNAPL 이 존재하는 환경에서 비활성 기체의 DNAPL 로의 상분배가 $^{3}H-^{3}He$ 연령 계산에 영향을 미칠 수 있음을 시사한다.

주요어: DNAPL, $^{3}H-^{3}He$ 연령 추적자, 비활성 기체, 상분배